



OPEN ACCESS

EDITED BY

Nan Wu,
Tongji University, China

REVIEWED BY

Wei Li,
Chinese Academy of Sciences (CAS), China
Entao Liu,
China University of Geosciences Wuhan,
China

*CORRESPONDENCE

Shiguo Wu

✉ swu@idsse.ac.cn

Dawei Wang

✉ wangdawei@idsse.ac.cn

RECEIVED 05 April 2023

ACCEPTED 26 May 2023

PUBLISHED 05 July 2023

CITATION

Chen W, Wu S, Wang D, Betzler C and
Ma Y (2023) Stratigraphic evolution
and drowning steps of a submerged
isolated carbonate platform in the
northern South China Sea.
Front. Mar. Sci. 10:1200788.
doi: 10.3389/fmars.2023.1200788

COPYRIGHT

© 2023 Chen, Wu, Wang, Betzler and Ma.
This is an open-access article distributed
under the terms of the [Creative Commons
Attribution License \(CC BY\)](https://creativecommons.org/licenses/by/4.0/). The use,
distribution or reproduction in other
forums is permitted, provided the original
author(s) and the copyright owner(s) are
credited and that the original publication in
this journal is cited, in accordance with
accepted academic practice. No use,
distribution or reproduction is permitted
which does not comply with these terms.

Stratigraphic evolution and drowning steps of a submerged isolated carbonate platform in the northern South China Sea

Wanli Chen^{1,2}, Shiguo Wu^{1,2,3*}, Dawei Wang^{1,2*},
Christian Betzler⁴ and Yongsheng Ma⁵

¹Laboratory of Marine Geophysics and Georesources of Hainan Province, Institute of Deep-sea Science and Engineering, Chinese Academy of Sciences, Sanya, China, ²Southern Marine Science and Engineering Guangdong Laboratory (Zhuhai), Zhuhai, China, ³University of China Academy of Sciences, Beijing, China, ⁴Institute of Geology, University of Hamburg, Hamburg, Germany, ⁵China Petrochemical Corporation, Beijing, China

Drowned carbonate platforms on passive margins present a paradox, because their great growth potential exceeds the typical rates of passive margin subsidence and any relative sea-level rise driven by long-term processes in the geologic record. In this study, manned submersible observations, sampling, and high-resolution acoustic data were used to investigate a drowned isolated carbonate platform cropping out at a water depth of 536–800 m in the northern South China Sea. Based on the results, the Early Miocene strata of the platform are grouped into three units (AU1, AU2, and AU3) that formed on the fault-created topography. The fault-created topography served as a template for the onset of the carbonate platform deposition and as a pedestal for the localization of backstepped platforms in response to accommodation space variations, primarily driven by rapid subsidence and eustatic rises during the Early Miocene. The Middle Miocene strata of the platform are grouped into four units (AU4, PU1, PU2, and PU3), exhibiting a general switch from dominantly aggrading to dominantly prograding platform margins, in tandem with the cessation of faulting. The biostratigraphy and established seismic–stratigraphic correlations indicate that the carbonate platform was submerged during the late Middle Miocene. The banktop consists of a heterozoan carbonate factory dominated by large benthic foraminifera and coralline algae. This facies was deposited during a time interval when summer monsoon-induced upwelling triggered heterozoan factory turnover in other carbonate platforms in the region, such as at well XK-1 (Xuande Platform). The asymmetric backstepping of the platform margins demonstrates that summer monsoon-driven currents influenced the platform drowning. Therefore, summer monsoon-induced upwelling was a major factor influencing platform drowning during the late Middle Miocene. Platform growth did not persist due to the high subsidence rate throughout the Late Miocene. This study provides new insights into the drowning mechanism of a Miocene carbonate platform in the northern South China Sea and a new seismic analog for other ancient, isolated platforms worldwide.

KEYWORDS

drowning mechanism, stratigraphic evolution, drowning steps, isolated carbonate platforms, northern South China Sea

1 Introduction

Isolated carbonate platforms (ICPs) are common in the geologic record and constitute one of the crucial targets for petroleum exploration in mature basins (Fyhn et al., 2013; Bashir et al., 2021; Hendry et al., 2021). Guyots are seamounts that formed at or above sea level and have a flat-top morphology owing to wave erosion (Staudigel and Clague, 2010). Many guyots were built of drowned shallow-water carbonates that rested on edifice basalt. Guyot tops were once at the surface, thereby reaching the photic zone, where they could be colonized by shallow-water carbonate builders. After carbonate growth phases and seamount subsidence, formation of shallow-water ICPs was common (e.g., Pacific region; Flood, 2001). Many ICPs later drowned, while others persevered and continued to grow to become modern ICPs (Courgeon et al., 2016). The long-term evolution of ICPs and drowning episodes leading to guyot formation have been the focus of several studies over the last few decades; however, the controlling factors remain unclear (El-Yamani et al., 2022; Petrovic et al., 2023). The internal architecture, onset, growth, and demise of guyots are determined by the biotic evolution, eustasy, volcanism, subsidence, and environmental variables (Courgeon et al., 2018). Because of their long distance from terrestrial input, the controlling factor of the terrestrial input is usually not considered. This results in better assessments of the factors regulating carbonate evolution.

Platform drowning is thought to be caused by a variety of interactive factors, including (1) an abrupt increase in accommodation space induced by rapid sea-level rise and subsidence exceeding the carbonate growth potential and flooding the shallow-water carbonate platform below the photic zone (Schlager, 1981; Petrovic et al., 2023), (2) a sharp decline in carbonate factory production associated with the degradation of environmental and climatic conditions, such as global anoxic events and excess of clastic and/or nutrient input (Sattler et al., 2009; Vu et al., 2017), and (3) strong current flow causing sediment removal and exclusion of sessile fauna (Hata et al., 2017; Betzler et al., 2021; Ling et al., 2021). Under pressure, the factory's surface area may frequently decrease and retreat to higher or more protected topographies to combat unfavorable environmental conditions or keep up with the swiftly rising accommodation space. In this case, the drowning of the carbonate system is only partial and reflected in the characteristic backstepping morphologies.

The formation and demise of ICPs are frequent in the geologic record; however, the processes involved in time periods of tens of millions of years have only recently been recognized and quantified. During the Cenozoic, a wide range of ICPs formed and evolved in the Indo-Pacific region. Various examples of Indo-Pacific carbonate platforms have been described, and the associated facies models and controlling factors have been published. In the Maldives, shallow-water carbonate production began during the Eocene when shallow-water carbonate banks were formed. Multiple carbonate development episodes were separated by periods of subaerial exposure and drowning events caused by eustatic sea-level shifts, bottom current activity, or Indian Monsoon activity (Betzler et al., 2013; Betzler et al., 2018; Lüdmann et al., 2022). In the Mozambique Channel (MC), shallow-water ICPs were first established on

volcanic substrates during diverse Cenozoic periods, ranging from the Paleocene to the Early Miocene (Courgeon et al., 2016). These carbonate platforms evolved during distinct phases, including tectonic deformation, volcanism, massive backstepping, and drowning periods.

Several submerged Cretaceous atolls are dispersed across hotspots of volcanism in the Pacific Ocean. For example, Resolution Guyot, one of these currently submerged atolls, has a platform top that is around 1,200–1,400 m below sea level (El-Yamani et al., 2022). This region's production of shallow-water carbonates began in the Late Paleocene, and the subsequent carbonate platform growth, which included periods of subaerial exposure, ended with its drowning during the Middle Eocene (Jenkyns and Wilson, 1999). Drowning incidents that affected Pacific guyots in the Late Cretaceous and Early Cenozoic are thought to be related to the shift of the Pacific Plate, which forced shallow-water carbonate platforms into unfavorable environmental conditions at low latitudes (Wilson et al., 1998). The wide range of geological processes governing the growth and submergence of ICPs from the Cenozoic show the sensitivity of these systems to changes in accommodation space and environmental conditions over relatively long time scales. To enhance our understanding of shallow-water isolated carbonate systems, additional case studies under different settings are required.

The northern continental margin of the South China Sea (SCS) is characterized by several distinct modern isolated carbonate systems (Figure 1). Aside from these coral islands, bathymetric grids show that several drowned ICPs crop out in waters hundreds of meters deep. Previous research has focused only on the architecture and evolution of modern carbonate platforms using seismic data and drilling wells on islands (Wu S. et al., 2020; Qin et al., 2022; Wu et al., 2022; Liu G. et al., 2023; Liu Y. et al., 2023). Several recent studies presented preliminary data on the lithostratigraphy and geochemistry of such wells (Wang et al., 2013; Shao et al., 2017; Chen et al., 2021; Wang R. et al., 2018; Wu et al., 2019; Wu et al., 2021a; Xie et al., 2008; Yang et al., 2022). However, the evolution and drowning mechanisms of submerged platforms in the northern South China Sea (SCS) have thus far received little attention. The Ganquan Plateau (GP) is the largest drowned ICP in the northern SCS; it is a suitable study site for amending the knowledge on drowned carbonate platforms, with recent oceanographic cruises having acquired multichannel seismic reflection profiles. Based on these data collected in 2017 and 2021, this study aims to (1) investigate the morphology, distinct seismic facies, and depositional geometries of the GP; (2) determine the timing, carbonate factory, and processes of platform drowning; (3) discuss the major episodes of platform growth and compare them with those in records of other ICPs in the Indian and Pacific Oceans; and (4) examine the interactions with regional subsidence, sea level, current, and other environmental factors.

2 Geological setting

The greatest marginal sea off East Asia is the SCS, created by seafloor spreading between 33 and 15 Ma (Briais et al., 1993; Li

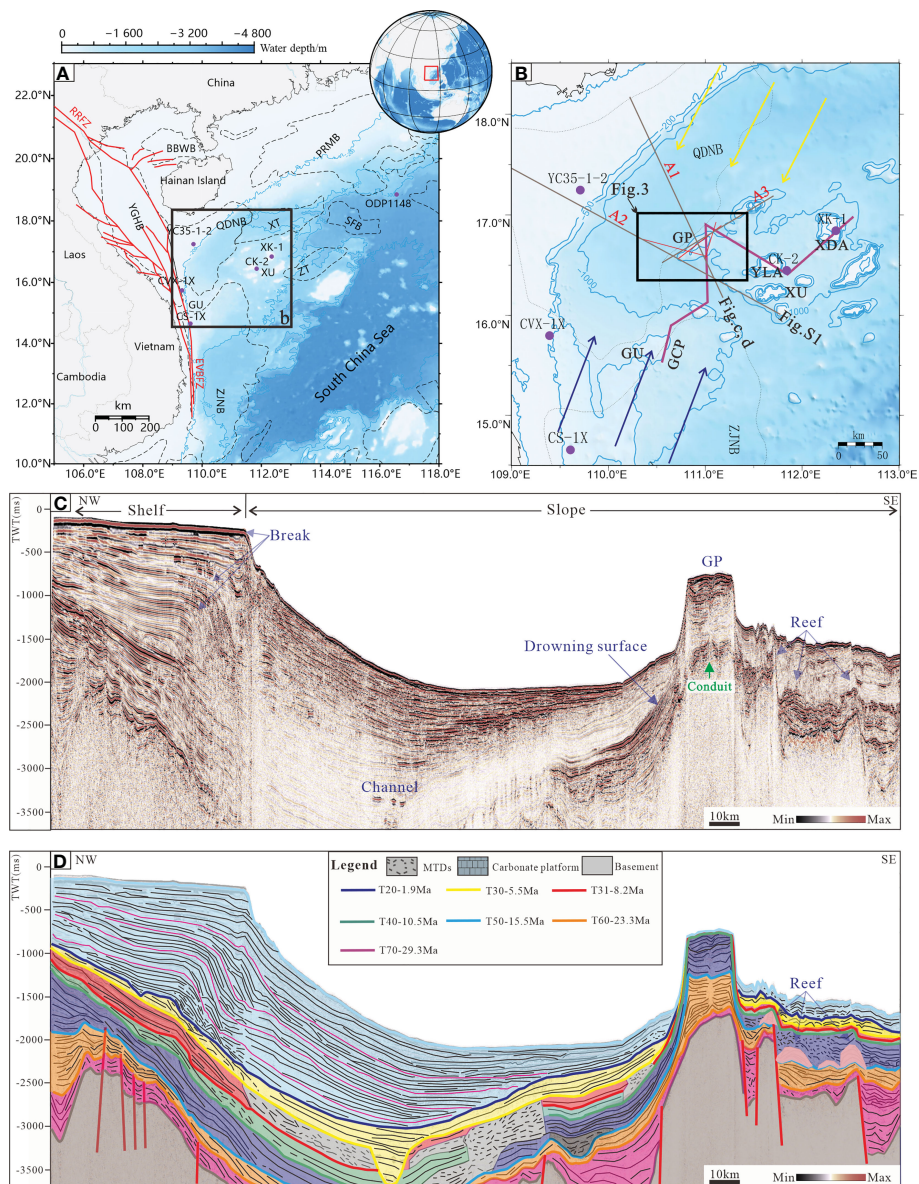


FIGURE 1 General geographic setting of the study. (A) Location map illustrating the regional bathymetric setting and the major Cenozoic basins in the study area. Structural outline modified after [Vu et al. \(2017\)](#). (B) Location of high-resolution 2D seismic data and wells used in this study. Yellow and blue arrows indicate the directions of winter and summer monsoon winds. Grey lines indicate the 2D seismic profiles discussed in the paper. The purple line is the location of the topographic profile. (C, D) NW–SE seismic section A1 over the continental shelf and slope showing the Qanquan Platform (GP) drowned during the late Middle Miocene (T40). Purple solid lines in sequence S1 represent the boundary of sub-packages bounded by the unconformities and seismic reflection terminations. The ages of seismic surfaces are based on the published stratigraphy from wells YC35-1-2 and CVX-1X ([Xie et al., 2008](#); [Wang et al., 2013](#); [Vu et al., 2017](#)). BBWB, Beibuwan Basin; YGHB, Yinggehai Basin (also named Song Hong Basin); QDNB, Qiongdongnan Basin; ZJNB, Zhongjiannan Basin (also named Phu Khanh Basin); GU, Guangle Uplift; GCP, Guangle carbonate platform; XU, Xisha Uplift; YLA, Yongle Atoll; XDA, Xuande Atoll; GU, Guangle Uplift; RRSZ, Red River Shear Zone; EVBF, East Vietnam Boundary Fault.

et al., 2015). The Xisha Uplift (XU) and its nearby depressions are the primary structural features in the northern SCS (Figure 1). The XU has experienced two stages of tectonic evolution: rifting and post-rifting thermal subsidence. Since the Late Cretaceous, the XU has experienced rifting, and its crest in the Early Miocene was fragmented into small, fault-controlled elevated blocks and intermediate grabens (Sun et al., 2003). The XU was submerged during the post-rifting thermal subsidence stage (23.3 Ma), and various biothermal carbonate platforms began to emerge on these

uplifts (Wang H. et al., 2018). According to well data, the basement rock of the XU is composed of granite, gneiss, and basalt, indicating the existence of regional metamorphism and magmatic activity. From the Late Miocene to the Quaternary, magmatic activity, i.e., volcanoes and intrusions, occurred at the XU and in the surrounding regions (Gao et al., 2019a).

Several tropical carbonate platforms and reefs comprising the Xisha Islands (Paracel Islands) have grown extensively on the XU. The studied GP, located on the western margin of the XU, is one of

these carbonate platforms. A 1,257 m thick carbonate succession that was penetrated by well XK-1 on the Xuande atoll shows that carbonate deposition in the XU started in the Late Oligocene (Wu et al., 2021b). In this study, we propose a stratigraphic model and depositional history of the GP based on the findings from well YC35-1-2 in the Qiongdongnan Basin (QDNB), wells CVX-1X and CS-1X at the Guangle Uplift (GU), and wells CK-2 and XK-1 at the Yongle and Xuande atolls (Figure 2). Seven formations were identified in the Cenozoic stratigraphic sequence in the QDNB and GU based on well data, seismic reflection characteristics, and seismic facies (Figures 1C, 2). The Oligocene to Miocene boundary (regional unconformity T60; 23.3 Ma) separates all strata into syn- and post-rift phases. Formation S1 is part of the syn-rift sequence, which is rarely found on carbonate platforms. Formations S2, S3, S4, S5, S6, and S7 were deposited during the post-rift period, when carbonate platforms were mostly formed (Figures 1C, 2). Chaotic or half-transparent reflectivity is evident in most of the QDNB area, suggesting that the mass transport deposits (MTDs) during the deposition of sequence S3 (upper Late Miocene), known also as Huaguang MTDs documented by Wang et al. (2013), were widely distributed (Figures 1C, D).

The East Asian Monsoon (EAM), which has been present since the Early Miocene, and possibly since the Eocene, governs the climatic and oceanographic settings of the Southeast Asian area (Clift et al., 2014; Loo et al., 2015). In the SCS, the East Asian Summer Monsoon (EASM) from the southwest dominates from May to September, whereas the East Asian Winter Monsoon (EAWM) from the northeast dominates from November to

March (Hu et al., 2000). The strong EASM wind triggers upwelling off the eastern Vietnam coast in summer, resulting in significant primary productivity with chlorophyll-a values ranging from 0.16 to 0.40 mg m⁻³ (Xie, 2003). These chlorophyll-a values imply mesotrophic to eutrophic conditions, which would limit or prevent coral growth and reef formation (Mutti and Hallock, 2003). Since the Late Eocene, the SCS has been affected by the EASM. This monsoonal effect increased during the Miocene, as the EASM began to intensify during the Early Miocene and was greatly strengthened during the Middle Miocene. Monsoon-induced upwelling from Vietnam's east coast is likely to have reached the Xisha Islands during the late Early Miocene and Middle Miocene, when the monsoon was at its peak (Clift et al., 2014; Wu et al., 2019). The EAWM is currently stronger than the EASM, and determines the modern facies distribution of atolls in the Xisha Archipelago (Wu S. et al., 2020). Surface circulation in the SCS is influenced by monsoon winds associated with the EAM. In summer, it has anticyclonic circulation, whereas in winter, it has cyclonic circulation (Hu et al., 2000).

3 Materials and methods

The multibeam bathymetric data utilized in this study were collected between 2008 and 2017 using a Kongsberg EM122 (frequency of 12 kHz) multibeam system. The data cover a large area of approximately 5,000 km², with the water depth values ranging between 300 and 1,500 m. The data were gridded with a

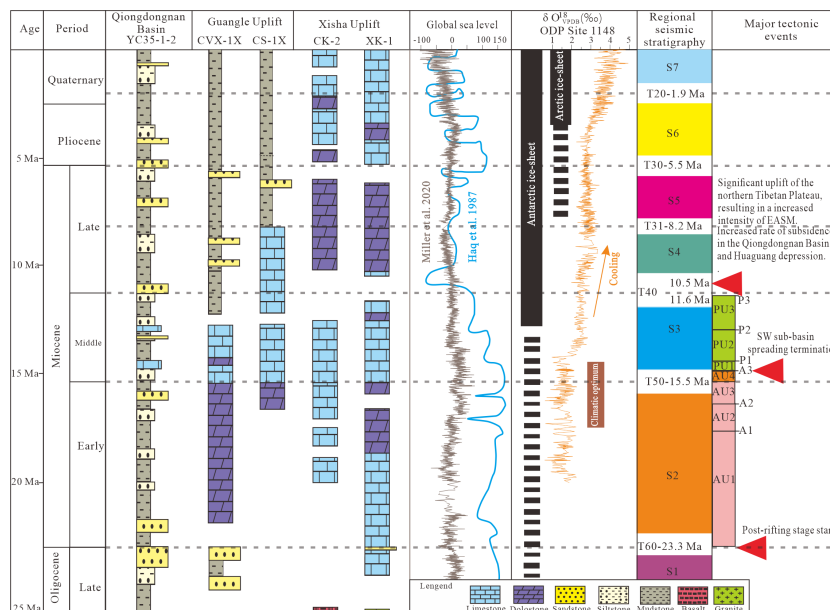


FIGURE 2

Chart summarizing the stratigraphic correlation and relevant Cenozoic global trends, including (i) lithostratigraphic correlation sections of five wells (YC35-1-2, CVX-1X, CS-1X, CK-2, and XK-1) from two uplifts and the QDN basin (The locations of the wells are indicated in Figure 1A. YC35-1-2 stratigraphy modified after Xie et al. (2008). CVX-1X and CS-1X stratigraphies compiled from Vu et al. (2017). CK-2 stratigraphy modified from Yang et al. (2022). XK-1 stratigraphy modified from Wu et al. (2019)); (ii) global eustasy (Haq et al., 1987; Miller et al., 2020); (iii) paleoclimate, including benthic δ18O at ODP site 1148 (Zachos et al., 2001; Zhao et al., 2001); (iv) stratigraphy, including regional interpretations of stratigraphy at the QDN basin, and Xisha and Guangle carbonate platforms; and (v) major regional tectonic events that impacted these areas.

cell size of approximately 100 m resolution and a vertical resolution of approximately 1.0–3.3 m. These data were useful for determining the undersea topography of the XU.

The three-manned submersible “*ShenhaiYongshi*” operated by the Institute of Deep-sea Sciences and Engineering, Chinese Academy of Sciences, was used for observations and sampling. Underwater videos and associated pictures were collected using an external color video camera on the submersible. Three carbonate samples were collected by the mechanical arm of the submersible. Two samples (C1, C2) were collected from the carbonate terraces at the platform top. One sample (C3) was obtained from the platform slope. Preliminary core observations and thin-section microscopic observations were performed using a polarizing microscope. The reconstruction of the carbonate depositional environments was based on the interpretation of biogenic assemblages and depositional textures. The results of this study were compared with previously published results on the biostratigraphy of wells XK-1 and CK-2 inferred from large benthic foraminifera (LBF) (Ma et al., 2018; Meng et al., 2022).

The 2D seismic data utilized in this study were collected in 2017 using six clustered mini-GI guns with a maximum output of 500 in3 and a 500-m long streamer with a trace spacing of 3.125 m. The seismic data had a frequency range of 10–1,000 Hz, with a dominant frequency between 100 and 120 Hz. Seismic data processing was performed using the GeoEast software. The Radon transform, surface-related multiple elimination, velocity analysis, and pre-stack time migration were all used for data processing (Wang J. et al., 2018). The 2D seismic data were interpreted using GeoEast 3.0.1. Seismic depth conversion was done using an average sonic velocity of ~2,500 m s⁻¹ for the coeval carbonates (Anselmetti and Eberli, 2001); this velocity and the dominant frequency suggested a vertical resolution of ~8 m in the data. The time depth conversion was completed on GeoEast and was based on the following equation: True Depth = ((TWT depth / 2) / 1000) × velocity.

4 Results and interpretations

4.1 General geomorphology

The GP is characterized by an overall flat-top morphology with a surface area of 310 km². This platform morphology extends over a distance of 45 km from northeast to southwest and over 12 km from northwest to southeast, and is characterized by an elongated shape following the SW–NE orientation of the XU margin (Figures 3A, B). The bathymetry of this platform top ranges from -800 to -536 m, whereas it rapidly decreases to -1,100 and -1375 m at the platform slope toe (Figures 3C–E). The platform top features several circular depressions of unknown origin. The overall morphology shows a pattern of stepwise shallowing from southwest to northeast. The southeastern platform margin is substantially more rugose than the northwestern edge, and has a higher declivity (Figures 3C–E). The flat-topped submarine morphology of the GP exhibits sharp and

abrupt margins that are commonly incised by well-developed, 2.1- to 8.7-km wide, steep convex-bankward embayments. The embayments are more pronounced on the southeastern flank of the GP most likely due to the platform margin collapses and slope failures affecting that area and resulting in a typical “scaloped” geometry of the bank margin. Rugged morphologies, irregular reliefs, and numerous circular structures are evident at the slope toe of the platform (Figure 3E). The northwestern flank of the platform exhibits two drowned terraces at depths of approximately 1,315 and 1,217 m (Figure 3E).

Coupled analyses of high-resolution bathymetric grids (Figure 3) and underwater videos (Figure 4) were used to determine the nature of the geological features. The platform top is characterized by flat, porous, and dull gray rocky slabs that are generally overlain by superficial sediments (Figures 4A, B), exhibiting common carbonate rock characteristics. Underwater images of the rugged morphologies and irregular reliefs revealed outcrops of bright rocks associated with vitreous texture and rounded rocky formations resembling pillow lavas, and dense polygonal fracturing networks that are similar to the tensional/contraction cracks that typically form during submarine volcanic eruptions (Figures 4C, D).

4.2 Carbonate samples

Two carbonate rock samples (C1, C2) were retrieved from two carbonate terraces of the platform top (Figures 4A, B; Table 1). The samples are approximately 2–3 cm thick (Figures 4E, F). Both samples have a dull grey color, owing to manganese oxide incrustations. The rocks are perforated by borings, which enlarged the cavities and fractures in the carbonate. Both carbonate samples comprise packstones marked by various shallow-dwelling carbonate producers, such as LBF and coralline algae (Figures 5A–D). Among the LBF, *Nephrolepidina* spp., *Amphistegina* spp., *Miogypsina* sp., *Planorbulinella larvata*, *Textularia* sp., *Operculina rectilata*, *Cycloclypeus* sp. are evident. The genus *Amphistegina* occupies the largest volume, followed by the genus *Nephrolepidina* (Figure 6). Among the identified coralline algae, Corallinales are the most abundant (Figures 5A, C). Hermatypic corals are generally rare in both samples. A facies of micritic packstone-bearing planktonic foraminifera overlies the Mn crust in sample C1, thereby recording the end of shallow-water carbonate production and the drowning of the carbonate platform below the euphotic zone (Figure 5B). The planktonic foraminiferal assemblages include *Globigerina* spp. and *Globigerinoides* spp.

A poorly lithified sample (C3) from the platform slope corresponds to skeletal floatstone-bearing coralline algae, planktonic foraminifera, and *halimeda* algae (Figures 5E, F). The planktonic foraminiferal assemblages include *Globorotalia* spp. and *Pulleniatina* spp. (Figure 5E). Among the identified coralline algae, Hapalidiales are relatively abundant (Figure 5F). Volcanic fragments are not evident in sample C3, suggesting the absence of exposed volcanic landforms on the southwestern flank of the platform at the time of deposition.

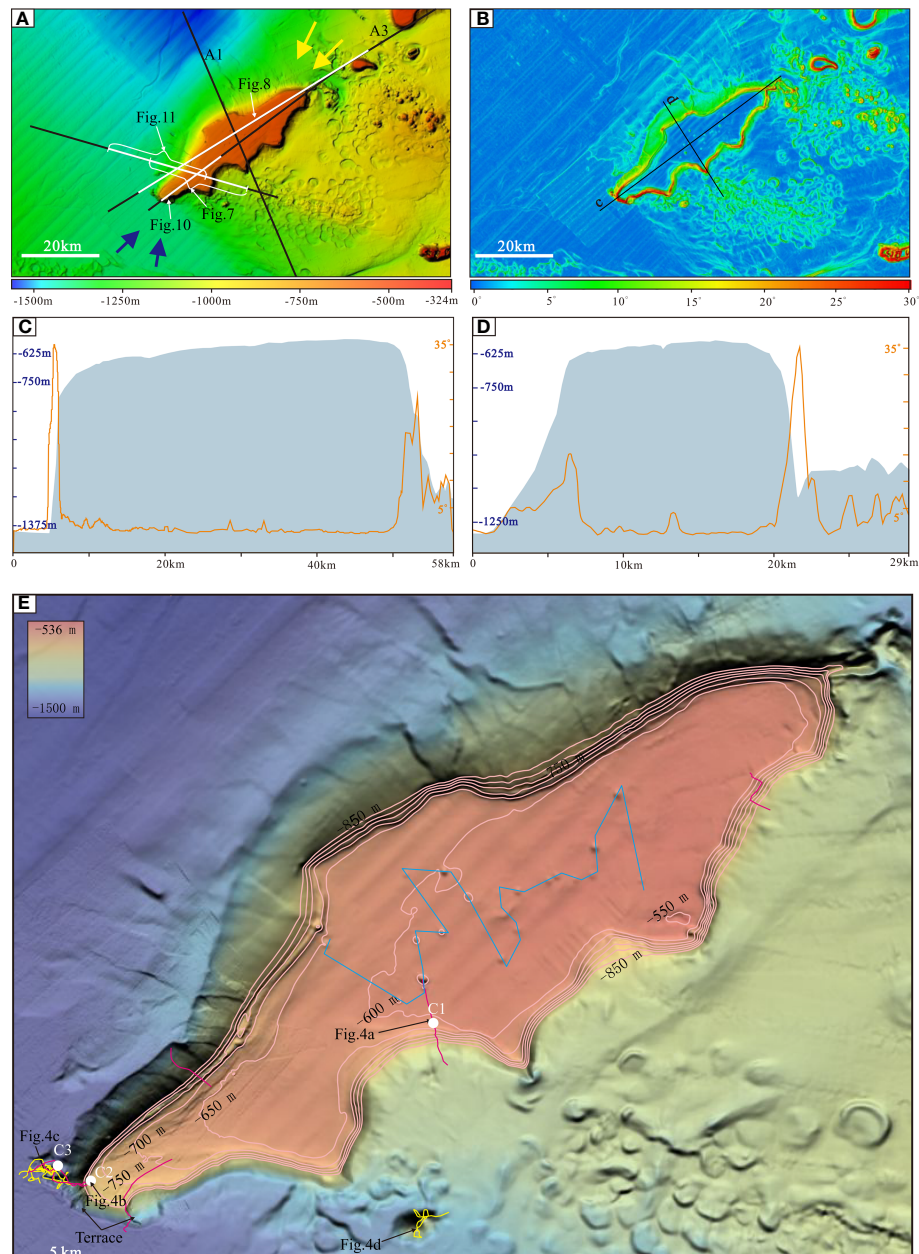


FIGURE 3

(A) Bathymetric map of the carbonate platform. White lines indicate the position of the seismic profiles. (B) Slope and steepness map of the area. Black lines indicate the cross-sections in panels c and d. (C) Bathymetric and slope profile across the platform (SW–NE direction) displaying a shallowing of the northeastern platform top. (D) Bathymetric and slope profile across the platform (NW–SE direction) displaying the steeper southeastern platform margin than the northwestern. (E) Close up of the GP occurring at 800 m depth. The blue solid line goes through all the pockmarks. White solid circles correspond to the locations of the samples collected by the submersible. Purple solid lines indicate dive tracks on the platform top, whereas yellow solid lines indicate dive tracks on the submarine volcanoes around the platform.

4.3 Seismic interpretation

4.3.1 Regional stratigraphic framework

A seismic profile (A1) spanning the northern continental shelf, QDNB, and GP allowed us to constrain the stratigraphic sequences of the GP based on our previously established seismic framework Wang et al., 2013; Wu S. et al., 2014, revealing the stratigraphic evolution relationships between the GP and adjacent basins. Eight key horizons related to the carbonate platform, including the

seafloor (T0, T20, T30, T31, T40, T50, T60, and Tg), were interpreted, and seven intervals (seismic sequences S1–S7) were identified within seismic profiles A1 and A2 (Figures 1; S1).

At regional unconformity T60, which marks the shift from syn- to post-rifting in the study region, carbonate platforms began to develop along with the formation of deep-water environments in the XU (Wu S. et al., 2014). Regional unconformity T50 is overlain by widely distributed carbonate deposits, and carbonate build-ups and reefs are established on the periphery of the carbonate system

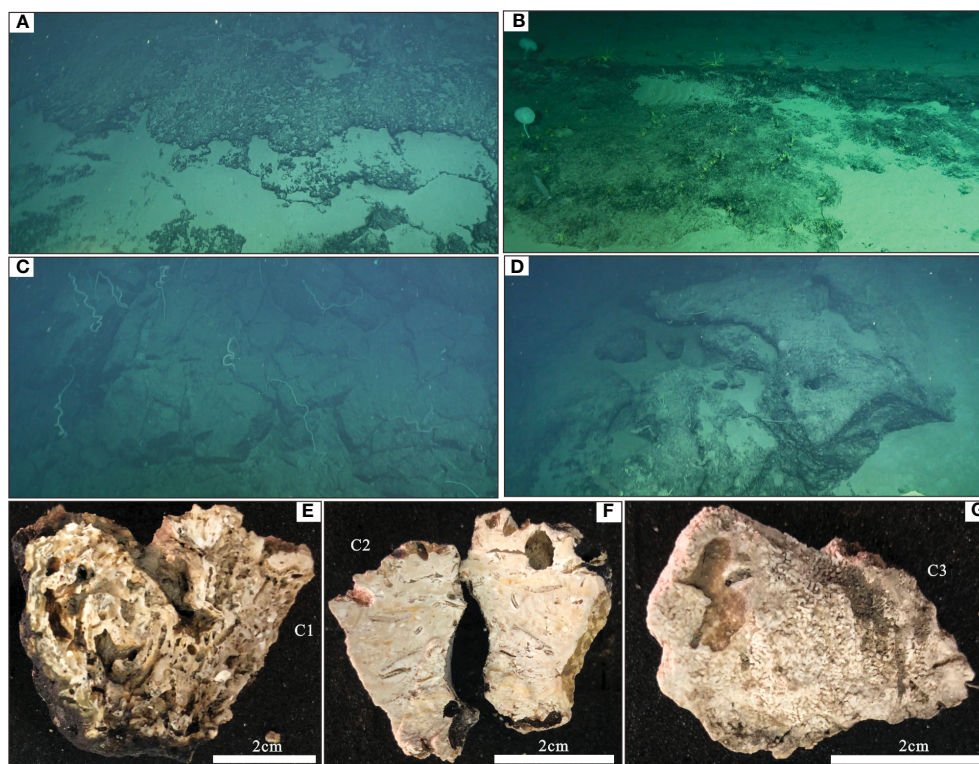


FIGURE 4

Sea bottom and sample pictures. (A, B) Reef carbonates along the backstepping platform margin. (C, D) Volcanic outcrops at the platform flank. See Figure 3E for the location. (E-G) Photograph of carbonate samples collected by manned submersible (see Figure 3E for the locations of the samples).

(Figure 1). Importantly, regional unconformity T40, which has a convex-up shape in comparison with the surrounding topography, correlates with the drowning surface of the submerged carbonate platform (Figures 1C, D). The progradational continental shelf is recognized within the study section, showing rapid Quaternary siliciclastic progradation, as documented by Xie et al. (2008). The GP is not buried by siliciclastic deposits and crops out at the sea floor (Figure 1). Gas hydrates near the GP were identified in the seismic images from the occurrence of bottom simulating reflectors (BSRs) in the QDNB (Figure S2).

4.3.2 Stratigraphic framework of the carbonate platform

The seismic characteristics of the GP carbonate platform are distinct from those of the nearby strata. Different seismic facies in the high-resolution seismic data span the entire platform-to-

basin transect. Table 2 summarizes the traits and examples of these images.

An inclined fault block with steep margins formed by normal faults supports the drowned carbonate platform, which is composed of sequences S6 and S5 (Figures 7–9). The topography of the tilted fault block is more pronounced in the southwestern portion of the platform, as shown in Figure 7. The lower carbonate succession (S6) lies between reflectors T60 and T50 and includes three seismic units (AU1, AU2, and AU3), backsteps on the northwestern margin, and aggrades on the southeastern margin (Figure 7). The basal unit AU1 lies above the northwestern margin of the northwestward-tilted fault block, is the thickest in the northwestern margin, and thins toward the higher southeastern margin (Figure 7). The initial presence of isolated carbonate build-ups on the northwestern margin of the tilted fault block contributed to the flat-topped morphology of the carbonate platform. The northwestern margin of the southwestern

TABLE 1 Synthetic table of biostratigraphy and nature of carbonate samples collected on the GP.

Sample	Lat/Long	Foraminifera Biostratigraphy	Depositional Environment	Depositional Texture Main components
C1	16.6413°N/110.9002°E	Middle Miocene	Shallow-water Carbonate platform	Packstone of LBF and RA
C2	16.5653°N/110.7331°E	Middle Miocene	Shallow-water Carbonate platform	Packstone of LBF and RA
C3	16.5761°N/110.7192°E	No data	Outer platform	Floatstone of PF, RA and Halimeda

PF, Planktonic Foraminifera; LBF, Larger Benthic Foraminifera; RA, Red Algae.

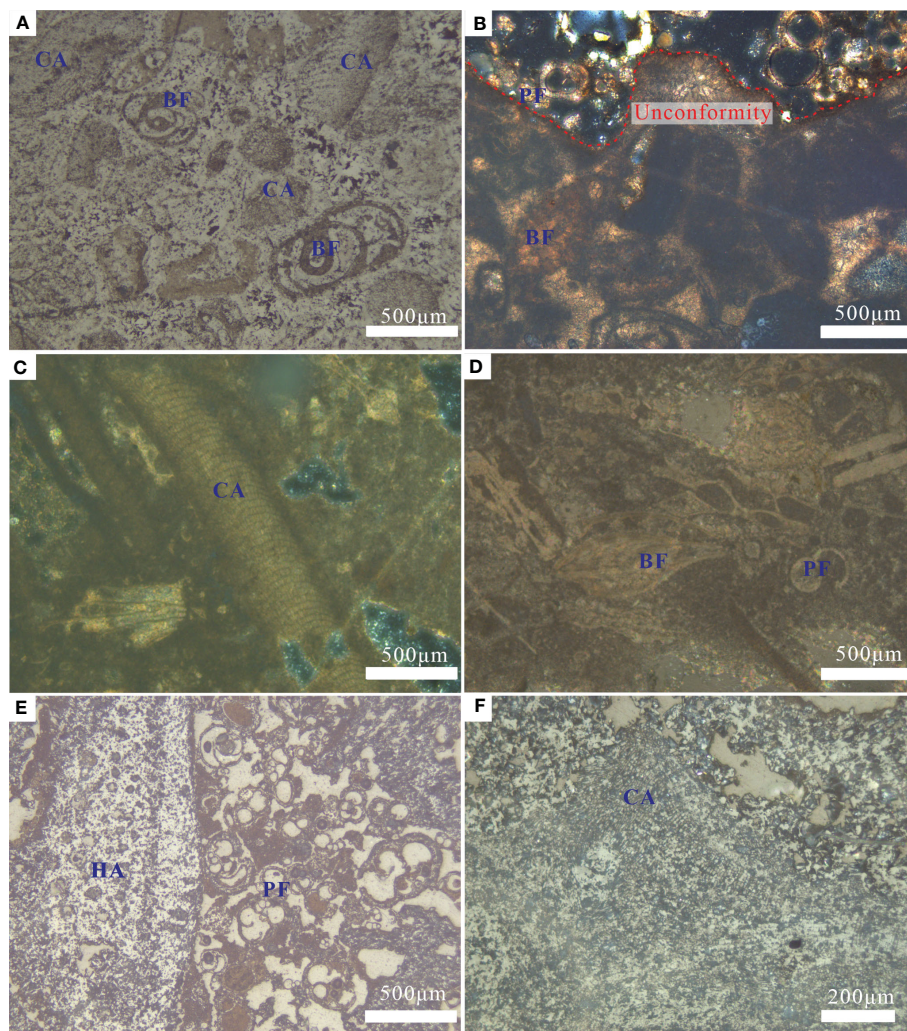


FIGURE 5

Thin sections micrographs. HA, Halimeda algae; PF, planktonic foraminifera; CA, coralline algae; LBF, large benthic foraminifera; (A) Packstone of CA and LBF. CA is characterized by corallinales; scale 500 μm , sample C1. (B) Erosive unconformity between boundstone of LBF and CA and packstone rich in PF; scale 500 μm , sample C1. (C, D) Packstone of CA and LBF. CA is typified by *Neogoniolithon* sp.; scale 500 μm , sample C2. (E) Floatstone of PF, CA and HA.; scale 500 μm , sample C3. (F) CA is typified by *Mesophyllum* sp.; scale 200 μm , sample C3.

part of the platform backstepped to the topographically high areas of the fault block at the top of AU2 and AU3 (Figures 7–9). AU1–AU3 are subdivided by surfaces (A1 and A2) defined by toplap below and onlap above, and are mappable across the platform.

The upper carbonate succession (S5), bounded by reflectors T50 and T40, consists of four seismic units (AU4, PU1, PU2, and PU3), marking a change from the backstepped to the aggradational and progradational northwestern margin (Figures 7–9). Most fault movements are interpreted to have stopped because of the offset of few faults by the end of AU4, and most margins exhibit aggrades in AU4 (Figures 7–10). The top of AU4 is a key boundary marking a switch from aggradational to progradational geometries of the carbonate platform. PU1, PU2, and PU3 are thicker along the northwestern flank of the platform than at the platform top. The deposits at the platform interior prograde northwestward and gradually decrease in thickness from PU1 to PU3. The three

seismic units have similar internal architectures, with repeated alternations between packages of tangential and sigmoidal reflections within the platform flank, and parallel to subparallel reflections within the platform interior. Convex-up or mound-shaped reflection areas (reef rim/mound seismic facies) are frequent at the margin of AU4 (Figures 7–10), while reef mounds are not observed at the margins of PU1, PU2, or PU3. The southeastern margin and flank exhibit aggradational geometries and erosional truncations (Figure 7), suggesting that margin collapses or slope failures occurred and contributed to the “scalped” margins. The aggradational and progradational margins are interpreted as windward (southeastern) and leeward (northwestern) margins, respectively, using the direction of progradation as evidence of leeward sediment flux. AU4–PU3 are separated by surfaces (A3, P1, P2, and P3) determined by truncation or toplap below and onlap above.

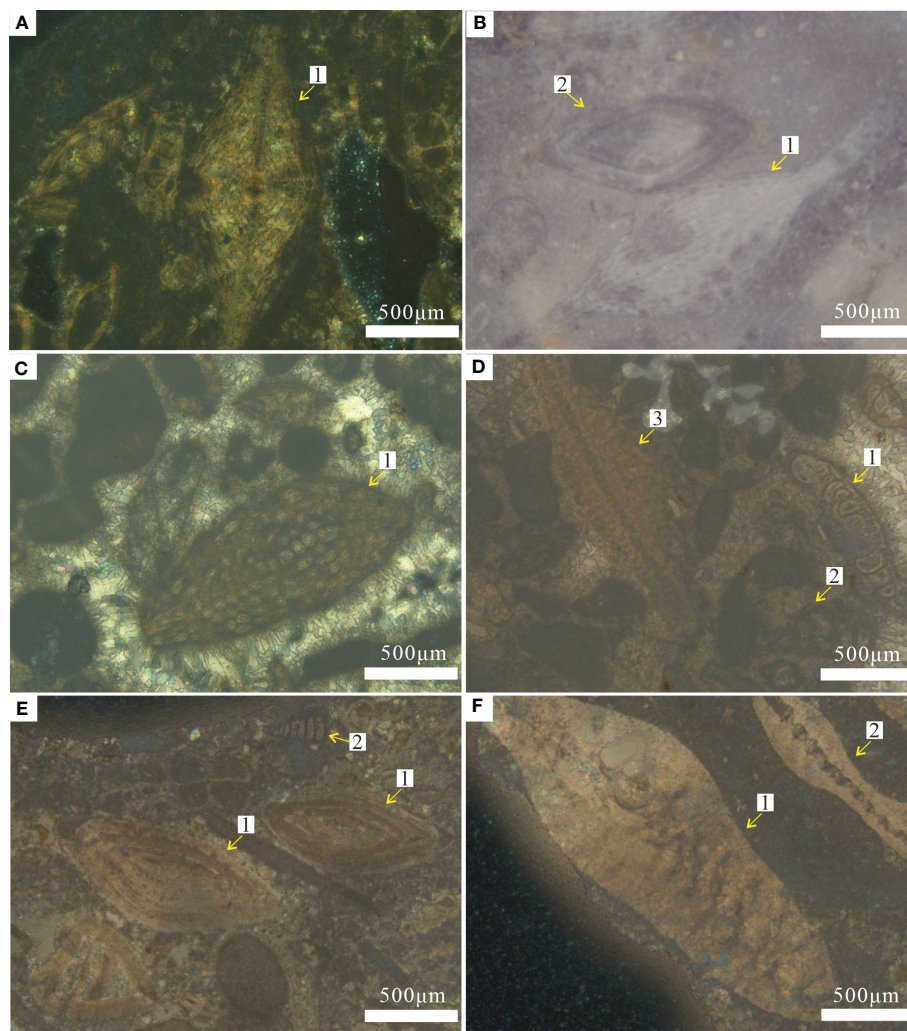



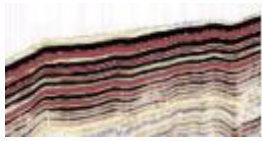
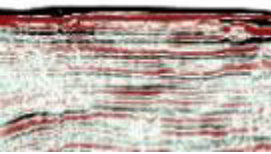
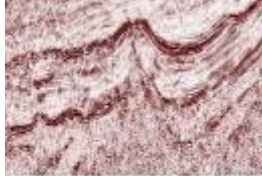
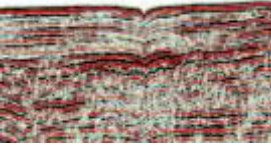
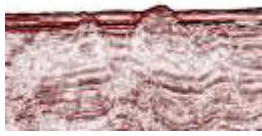
FIGURE 6 Photomicrographs of large benthic foraminifera. **(A)** *Nephrolepidina verbeeki*(Newton et Holland);scale 500 μm, sample C2; **(B)** 1: *Nephrolepidina* sp.; 2: *Amphistegina* sp.; scale 500 μm, sample C2. **(C)** 1:*Miogypsina* sp.;scale 500 μm, sample C1. **(D)** 1: *Planorbulinella larvata* (Parker & Jones); 2: *Textularia* sp.;3: *Nephrolepidina* sp.; scale 500 μm, sample C1. **(E)** 1: *Amphistegina* sp.; 2: *Textularia* sp.; scale 500 μm, sample C2. **(F)** 1:*Operculina rectilata* Cole; 2:*Cycloclypeus* sp.; scale 500 μm, sample C2.

TABLE 2 Seismic facies description and interpretation.

	Seismic facies	Reflection characteristics	Interpretation		Seismic facies	Reflection characteristics	Interpretation
SF1		sheet or wedge, downlap of lower reflection terminations, sigmoid reflection, low to high amplitude	sigmoid slope	SF6		margin backstepping	platform margin, shrinking
SF2		wedge, downlap of lower reflection terminations, tangential reflection, low	tangential slope	SF7		wedge, parallel to sub-parallel sigmoid reflections, showing offlap, as well as onlap and downlap, medium to high	drift

(Continued)

TABLE 2 Continued

	Seismic facies	Reflection characteristics	Interpretation		Seismic facies	Reflection characteristics	Interpretation
		to high amplitude				continuous, low to medium amplitude	
SF3		convex-up shaped mound, strong upper reflection, internal reflection are chaotic	reef rim/mound	SF8		sheet, parallel to sub-parallel reflections, medium to high continuous, low to high amplitude	basinal hemipelagics
SF4		sheet or wedge, parallel and sub-parallel reflection, continuous and semi-continuous, low to high amplitude	platform interior, lagoonal deposits	SF9		narrow, vertically elongated pipe-like shape, internal reflection are chaotic, low amplitude	magmatic intrusion
SF5		depression, layers below the depression are chaotic, disrupted and highly broken	fluid flow, seismic pipe, pockmark	SF10		convex reflector, parallel to sub-parallel reflections, low to high continuous, medium to high amplitude	sedimentary layers pushed up by the fluid flow

4.3.3 Synchronicity of platform backstepping and progradation

Three backsteps with backstepping distances of 1.8, 3.1, and 11.9 km, respectively, are evidenced by three wide terraces cropping out at water depths of 750.5, 680.3, and 612.5 m (Figure 10). The surfaces of the backsteps correspond to the seismic sequence boundaries separating PU1 to PU3. In the first step, the southwestern platform was initially submerged, and the platform margin backstepped to the terrace at a water depth of 750.5 m (Figure 10). Carbonate sample C2, obtained from this terrace, is composed of coralline algae and large benthic foraminifera (Figures 5C, S), suggesting that a heterozoan carbonate factory dominated the platform during the first step. In the second step, the southwestern platform margin backstepped further to the terrace, which lies at a water depth of 680.3 m (Figure 10). In the third step, the southwestern platform margin backstepped most significantly to form a terrace at a water depth of 612.5 m (Figure 10). The fossil assemblages on this terrace indicate that heterozoan carbonates thrived during the third step (Figures 5A, B).

The maximum thicknesses of PU1, PU2, and PU3 within the platform interior are 0.122s TWT (ca. 152.5 m), 0.077s TWT (ca. 96.25 m), and 0.061s TWT (ca. 76.25 m), respectively. The thicknesses of the seismic units are inversely proportional to the backstepping distances of the southwestern margin. Surface T40 represents the last backstepping surface characterized by a submarine high, with the top lying at a water depth of 536 m (Figures 3, 10). This submarine high is spindle-shaped (Figure 3). Furthermore, the platform backstepped more significantly on the southwestern side than on the northwestern side.

4.3.4 Post-S5 deposits

The platform-drowning surface is a continuous reflection with an intermediate to high reflection amplitude, exhibiting onlap by drift sedimentation at the platform flank (Figures 7–9). The internal architecture of the post-S5 deposits is characterized by a basal package of parallel to subparallel reflections and a slope package of parallel to subparallel sigmoid reflections with offlapping, onlapping, and downlapping geometries (Figure 8). A sediment body with drift facies characteristics evolves into basinal hemipelagics toward the basin on the western slope of the drowned carbonate platform (Figures 7–9). *In situ* carbonate production is thought to be an important factor controlling drift bodies (Reolid et al., 2019). Drift facies are uncommon on the southeastern platform flank, although they occur on the flanks of the volcanoes northeast of the platform (Figure 8).

4.3.5 Structures associated with magmatism and hydrothermal fluid flows

Several seismically transparent bodies connected to the basement are evident within the platform. They are characterized by a narrow, vertically elongated pipe-like shape with low amplitudes of seismic reflections, which is known as “pipe” structure. Tubular shapes are commonly imaged as transparent regions compared to the surrounding sedimentary layers or basement. This transparency suggests that they consist of materials with high scattering, such as sheeted dikes, and represent conduits from a deep magma reservoir. Twenty-one craters with diameters of 0.4–0.9 km and depths of 2–48 m were stacked on the pipes (Figure S2), and densely populated pockmarks developed at the northeast and east of the platform, with

larger diameters of 0.5–1.3 km and depths of 20–120 m, as calculated by Gao et al. (2019a). Correspondingly, the volcanoes around the platform were observed using submersible and seafloor bathymetric data (Figures 3, 4). In addition to the obvious intrusions forming the volcanic ridges, we detected several more “blind” intrusions buried within the sedimentary layers in the platform flank (Figures 8, 11), and the QDNB where the seafloor is paved by rapid sedimentation (Figure S1). The intrusive bodies are capped by convex reflections, indicating that the sedimentary layer is pushed up by the upwelling flow (blue arrows in Figure 11). The seafloor is also penetrated by convex reflections, and the pipes observed in these strata are pathways of the upwelling flow reaching the modern sea bottom (green arrows in Figure 11).

5 Discussion

5.1 Stages of platform evolution

The stratigraphic evolution of the GP can be divided into three distinct stages: (1) platform initiation and structurally controlled

retrogradation at the tilting margin (Figure 12, AU1–AU3; Figure 13A), (2) platform aggradation and cessation of faulting (Figure 12, AU4, Figure 13B), and (3) platform progradation and backstepping (Figure 12, PU1–PU3, Figures 13C, F, E). Finally, the platform drowned (Figure 13F). The strata deposited during stage 1 feature an evident northwestern margin retrogradation at the southwestern portion of the platform, suggesting that faulting may have remained active during this phase of deposition. The deceleration in accommodation production caused by the decreased fault-induced subsidence resulted in the occurrence of aggradational geometries in most of the platform margin during stage 2 (Figures 12, 13B). Reef mounds were commonly pronounced at the platform margin, indicating that frequent photozoan carbonate factory with greater growth potential likely dominated the platform during stages 1 and 2. The corresponding time periods were characterized by high sedimentation rates recorded by both wells XK-1 and CK-2 (Figure 12) (Yi et al., 2018; Fan et al., 2019). The photozoan carbonate factory reflected by the platform geometry is consistent with the frequent occurrence of photozoan carbonates from the Early Miocene (stage 1) to early Middle Miocene (stage 2) observed in well XK-1 (Wu F. et al.,

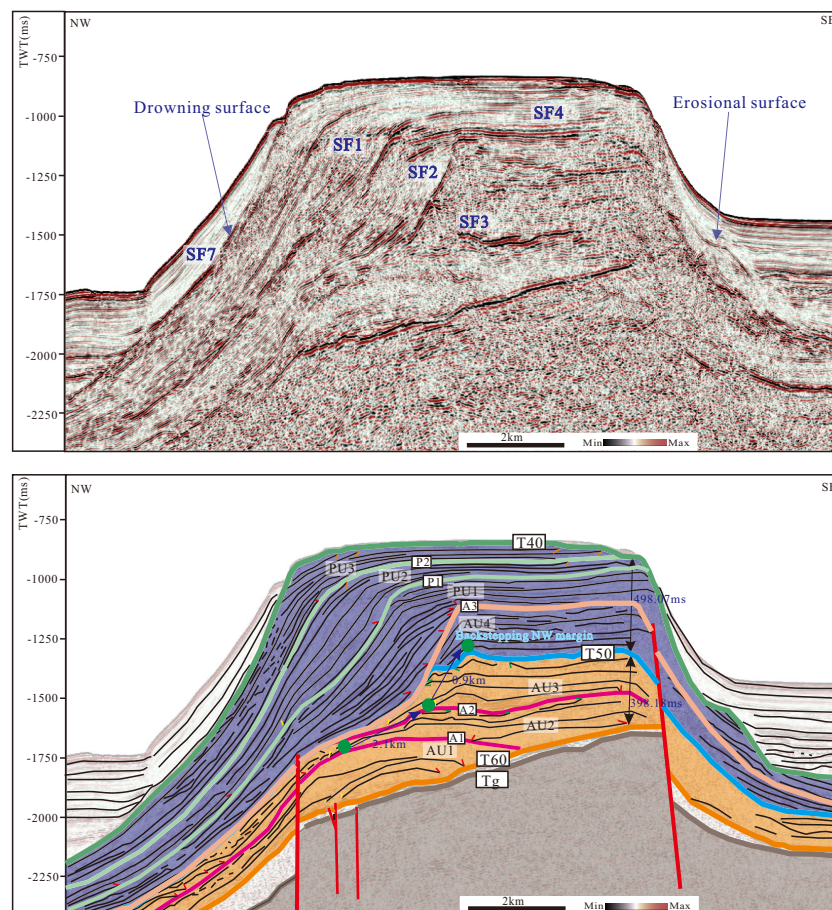


FIGURE 7 NW–SE seismic section across the GP and corresponding stratigraphic interpretation showing the growth and demise of the carbonate platform. In the former, green arrows highlight tubular transparent bodies (pipes), indicating volcanic conduits. In the latter, tics indicate the key stratal terminations: orange is truncation; yellow is downlap; green is toplap; and red is onlap. Faulting activity terminates owing to a few fault offsets by the end of AU4. Figure 3A for location.

2019). Most ICPs throughout the Indian and Pacific Oceans (Table 3), such as the Maldives, Yadana Platform, and Marion Platform, were dominated by photozoan carbonate factories with great growth potential during these two periods, and platform drowning generally occurred in active tectonic settings, such as the Yadana Platform (Table 2) (Paumard et al., 2017).

Stage 3 documents the synchrony of platform backstepping and progradation, which contradicts the sea-level process of stratigraphic stacking patterns. Previous studies have also documented the synchrony of drowning and ongoing bank-margin growth, which is contradictory to a sea-level explanation (Aubert and Droxler, 1996; Betzler et al., 2013). It is proposed that the cessation of normal faulting may have instigated platform progradation during stage 3, and that these backsteps may have been driven by changing environmental conditions. Coincident with the progressive reduction in stratal thickness from PU1 to PU3, the sedimentation rates recorded in wells XK-1 and CK-2 steadily declined (Figure 12). According to the combined analysis of carbonate samples and platform geometry, the reduction in carbonate production was caused by carbonate factory turnover from a photozoan to a heterozoan type. The platform shifted from

aggradation to progradation, and a change in faunal association occurred at 15 Ma on the Middle Miocene Maldives Platform (Reolid et al., 2019; Reolid et al., 2020). Similar examples can also be found in other carbonate platforms, where platform drowning was accompanied by changes in the carbonate factory toward a heterozoan type (Table 3). Furthermore, the platform backstepped more significantly on the southwestern side than on the northeastern side (Figure 13E). Therefore, platform growth has been asymmetric since the onset of platform drowning when the partial platform drowned. Most areas of the platform margins aggraded, and growth continued through progradation and slight aggradation. Similarly, the asymmetric growth of the Maldives carbonate platform also occurred during the partial bank demise with the synchronicity of continued bank-margin growth (Betzler et al., 2013).

The GP carbonate platform nucleated on a structural high and formed a spindle-shaped drowned bank in the last step of platform drowning (Figure 13F). According to Zampetti et al. (2004), a buried, drowned Miocene carbonate bank offshore Malaysia has a similar geometry and transitioned from flat-topped during the active growth stage to mound-shaped during the predrowning

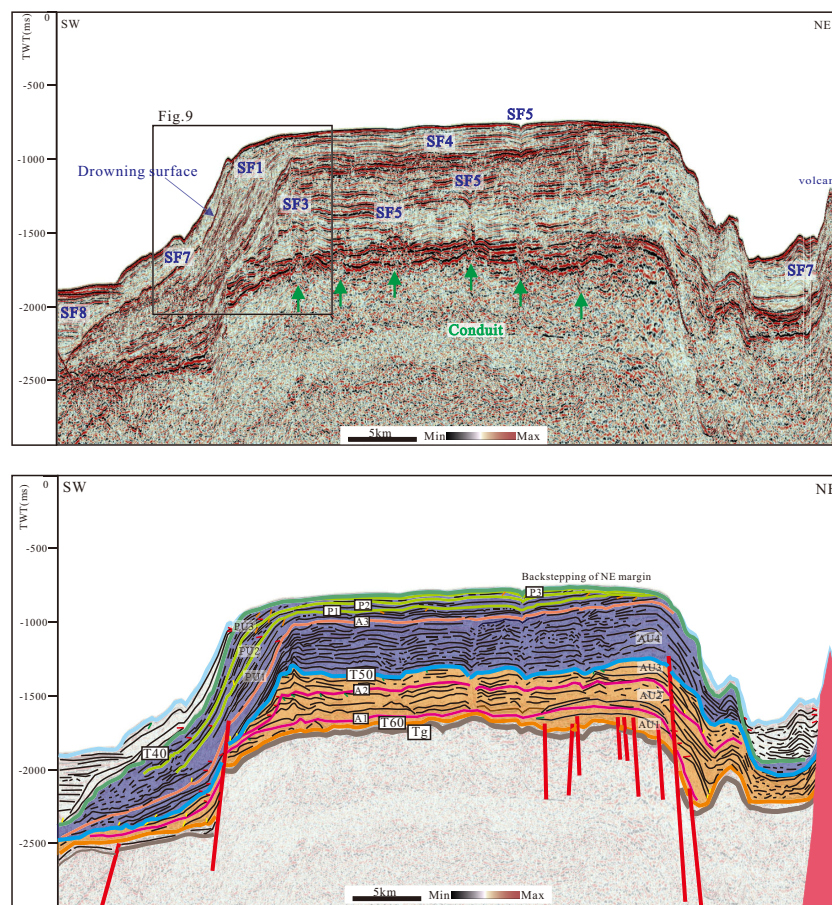


FIGURE 8 SW-NE seismic section across the GP and corresponding stratigraphic interpretation showing the growth and demise of the carbonate platform. In the former, the green arrows highlight tubular transparent bodies (pipe) indicating volcanic conduits. In the latter, tics note key stratal terminations: orange = truncation, yellow = downlap, green = toplap, and red = onlap. Prominent depression in the top-platform surface marks a giant collapse structure in the underlying carbonate succession. See Figure 3A for location.

stage. [Betzler et al. \(2009\)](#) also identified a spindle-shaped drowned bank that formed during the last drowning step of the partial drowning of the Maldives carbonate platform. This was viewed as the final phase of the subphotic mound development and submergence below the wave base. During the final drowning process of the GP, a similar evolution is thought to have generated a spindle-shaped drowned bank. Seismic stratigraphy and biostratigraphy suggest that the platform was submerged during the late Middle Miocene. The drowning surface of the GP was identified on the carbonate slope ([Figures 1, 7, 8](#)), corresponding to sequence boundary T40 (top of the Middle Miocene), which was recognized in our previous study on the continental shelf and QDNB ([Wang et al., 2013; Wu S. et al., 2014](#)). The foraminiferal assemblage of the two carbonate samples from the platform top was dominated by larger benthic foraminifers, such as *Nephrolepidina*, *Amphistegina* and *Miogypsina* ([Figure 6](#)), corresponding to the Middle Miocene foraminiferal assemblage also recorded in wells XK-1 and CK-2 ([Ma et al., 2018; Meng et al., 2022](#)). The last occurrence of *Nephrolepidina* and *Miogypsina* at 577.04 m depth in well XK-1 represents the top of the Middle Miocene ([Figure 12](#)) ([Ma et al., 2018](#)). [Boudagher-Fadel and Banner \(1999\)](#) defined the top of the Middle Miocene using the last occurrence of *Nephrolepidina*. Furthermore, the water depth at the highest point of the submerged platform was 536 m, falling within the depth interval

of the Middle Miocene tops (521–577 m) indicated by the wells ([Figure S3](#)). The seismic profile crossing the highest basement of the GCP also shows that the depth of the Middle Miocene top was 562 m ([Fyhn et al., 2013](#)), implying that the last drowning phase of the GP occurred during the late Middle Miocene.

5.2 Controlling factors of platform evolution

Inorganic nutrient availability, siliciclastic supply, sea-surface temperature, and relative sea level are the major factors controlling carbonate factory turnover, and platform growth and demise ([Mutti and Hallock, 2003; Halfar et al., 2006; Fyhn et al., 2009; Betzler and Eberli, 2019; Wu et al., 2019](#)). The aggradational and retrogradational platform margins reflect an increase in accommodation in stages 1 and 2. In such a scenario, relative sea-level changes appear to be the most probable major controlling factor of platform development. The backstepping of the platform margins toward topographically high areas was likely controlled by fault-induced subsidence during stage 1 ([Figure 7](#)). The inclined fault block, which remained topographically high, may have been controlled by younger faults that continued to move. The rising global sea level is also thought to have played a dominant role in shaping the platform geometries. Both global and local relative sea

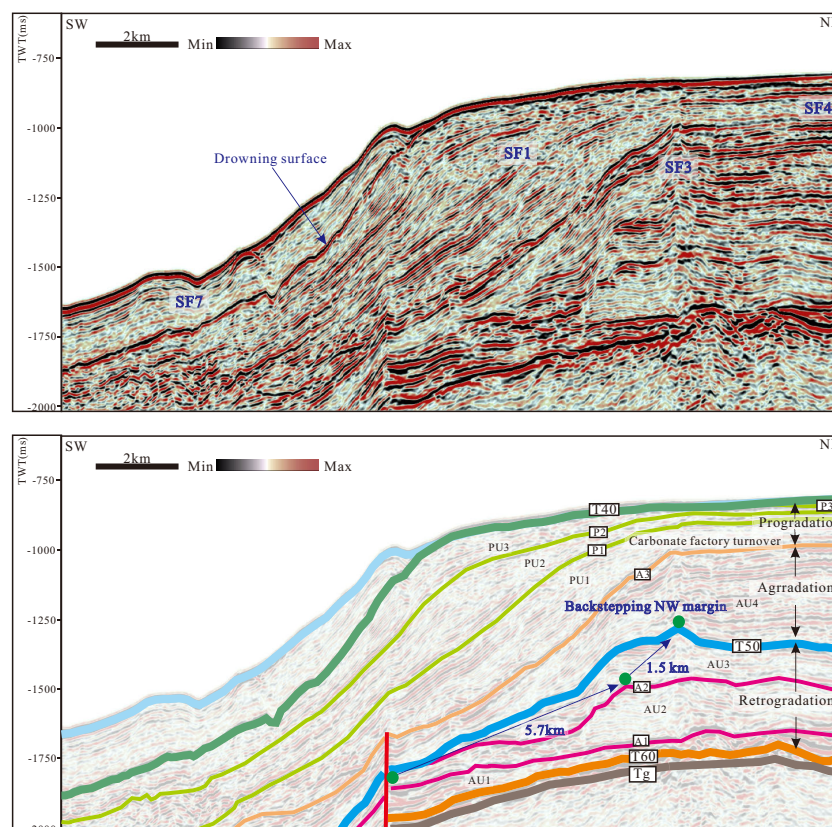


FIGURE 9

SW-NE seismic section across the northwestern margin of the GP showing the development of the platform margin. Faulting activity terminates due to few fault offsets at the end of AU4. See [Figure 3A](#) for location.

level curves indicate a rapid sea-level rise during the Early Miocene (Haq et al., 1987; Shao et al., 2017; Miller et al., 2020), and seismic data also indicate that the carbonate platforms were typically restricted to topographic highs on the XU due to the sea level rise during the Early Miocene (Wu S. et al., 2014). High sedimentation rates were recorded in both wells XK-1 and CK-2, demonstrating that carbonate production was likely high enough to be impacted from the high-frequency relative sea-level rises during the Early Miocene and early Middle Miocene (Figure 12). We suggest that optimal conditions for carbonate production and accumulation existed during these time intervals, compared with the growth rates of other carbonate platforms (Schlager, 2000; McNeill, 2005).

Platform progradation and backstepping were synchronous as a consequence of faulting cessation and summer monsoon-driven currents during stage 3. On the one hand, the faulting cessation may have triggered platform progradation. It has been proposed that the apparent chronological synchronicity between the faulting cessation and progression is partly due to a slowdown in accommodation production caused by a reduction in fault-induced subsidence. Previous studies have also documented that the faulting cessation

is coincident with the initiation of the expansion and coalescence of the Segitiga Platform caused by progradation, thereby demonstrating that the deceleration of accommodation production driven by decreased fault-induced subsidence contributes to platform progradation (Bachtel et al., 2004). The shallow-water components were also likely transported off the platform by summer wind-driven currents, resulting in platform progradation during stage 3. According to Clift et al. (2014), the EASM intensified over long periods from 21.2 to 17.3 Ma and from 15.6 to 10.5 Ma, with some oscillations occurring in each era. The heaviest summer monsoon formed between 15.6 and 10.5 Ma (Clift et al., 2014) and dominated the entire stage 3. On the other hand, the previous fault-induced subsidence and summer monsoon-driven currents, are also believed to have been responsible for the pronounced backstepping distance and the area on the southwestern side of the platform (Figures 13C–E). Heterozoan carbonates were found on the terraces caused by the gradual backstepping of the platform (Figure 5), indicating that favorable platform growth conditions deteriorated during stage 3. The stepwise drowning of the carbonate platform, coupled with a

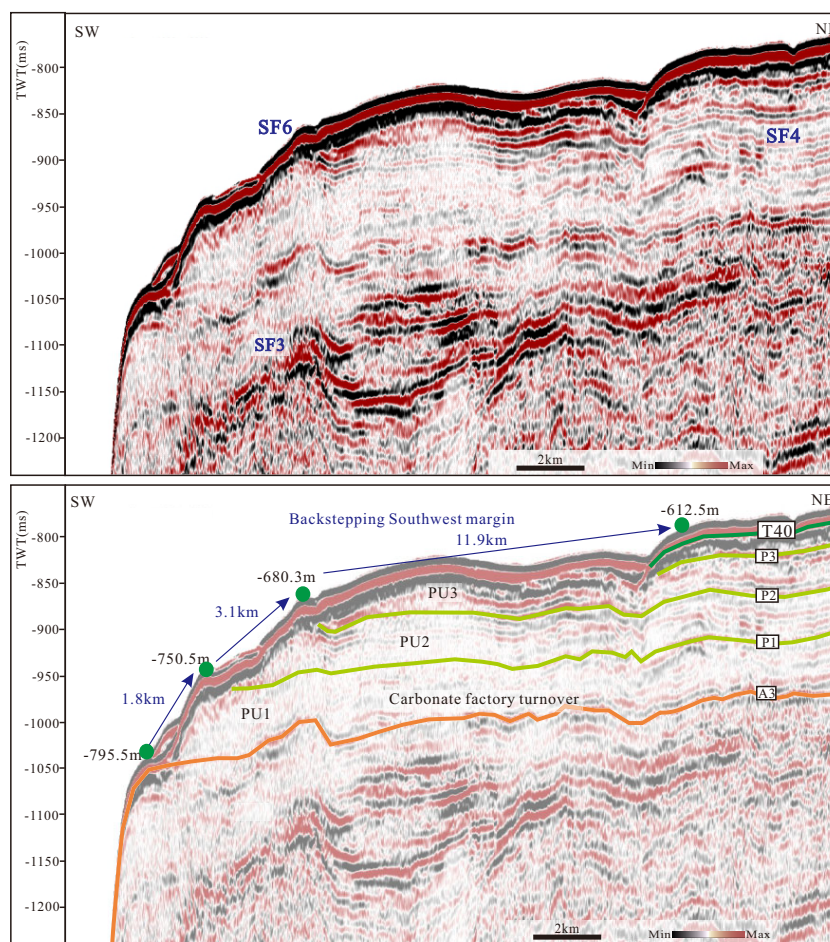


FIGURE 10

NW–SE seismic section across the southwestern margin of the GP showing that the backstepping margins are coincident with the progradational margins in Figures 10, Figures 11. The depths of the backstepping surfaces were determined using a sea-water velocity of 1,500 m/s where backstepping surfaces crop out at the seafloor. See Figure 3A for location.

steady decrease in stratal thickness from PU1 to PU3 and carbonate factory turnover from a photozoan to a heterozoan type (Figure 12), reflects the long-term worsening of platform growth conditions. According to data from well XK-1 analyzed by Wu et al. (2019), upwelling from the east coast of Vietnam caused by the EASM increased the nutrient influx, inhibited coral growth, suppressed the development of reef-related facies, contributed to the development of open bank facies and thus promoted carbonate factory turnover from a photozoan to a heterozoan type during the Middle Miocene in the Xuande Platform (Figure 12). Strong summer monsoon-related upwelling is also an inhibiting factor of the continued growth of the Phan Rang Carbonate Platform near the east coast of Vietnam (Fyhn et al., 2009). Betzler and Eberli (2019) compiled a list of modern and ancient examples of ICPs and carbonate contourite drifts documenting monsoon-triggered currents as a common element of carbonate platform drowning during the late Middle Miocene. The GP is closer to the east coast of Vietnam relative to the Xuande Platform (Figure 1); thus, the monsoon-induced upwelling zone could also reach the GP during the Middle Miocene. As a result, we believe that summer monsoon-triggered currents suppressed coral reef formation by generating topographical upwelling on the southwestern side of the platform, leading to the gradual occurrence of a heterozoan carbonate factory

with low growth potential on the carbonate terraces. These carbonate terraces on the southwestern side of the platform usually do not get affected by the relative sea-level rise resulting from the fault-induced subsidence, thereby leading to stepwise drowning of the GP. In addition, because of an abrupt increase in the subsidence rate detected in the surrounding QDN Basin (Wu S. et al., 2014; Zhao et al., 2018), the sustained coral reef ecosystem was probably completely destroyed by the subsequent enormous subsidence rate during the Late Miocene. The enormous Huaguang MTDs expanded synchronously into the examined area, indicating an unstable basement throughout this time period (Wang et al., 2013). Therefore, the shallow-water carbonate builders on the GP were unable to persist and became as visible as those on the Xuande and Yongle Platforms.

Although the oxygen isotope records from the Deep Sea Drilling Project and Ocean Drilling Project cores show warmer temperatures during the Early Miocene and a general decrease in temperature from the Middle Miocene (mid-Miocene climatic optimum) to present (Figure 2) (Zachos et al., 2001; Zhao et al., 2001), the significant abundance of photozoan carbonates during the Quaternary suggests that the temperature in the Xisha region has been sufficiently high since the Early Miocene for the production of photozoan carbonates (Wu et al., 2019). Therefore,

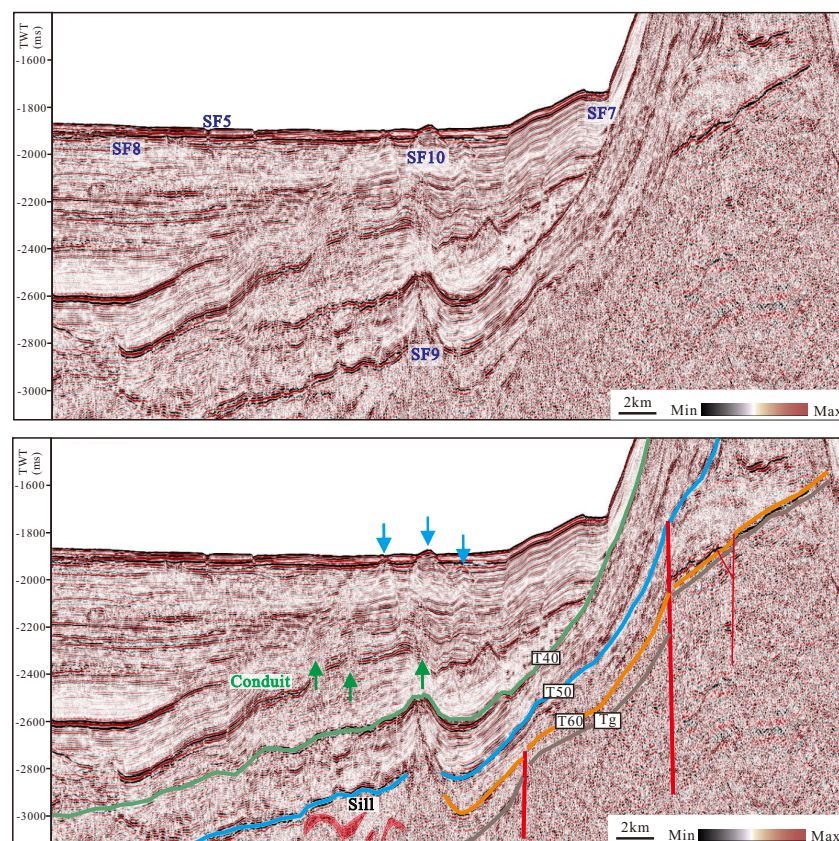


FIGURE 11

Seismic section around the GP showing the magmatic intrusions that occurred in this area. This image highlights tubular transparent bodies indicating volcanic conduits (indicated by green arrows). Upwardly convex reflectors are interpreted to be sedimentary layers pushed up by the upwelling flow (blue arrows). See Figure 3A for location.

the development of heterozoan carbonate factories and the subsequent platform flooding during the late Middle Miocene were not considered to be caused by a cooling event. Furthermore, the scarcity or absence of planktonic foraminifera indicated that heterozoan carbonates were deposited in shallower waters (Figure 5), implying that the occurrence of heterozoan-dominated carbonates during platform drowning was not caused by an increase in water depth during the late Middle Miocene. The drop in temperature and increase in water depth have also been recognized as less important drivers for the emergence of a heterozoan carbonate factory, as well as photozoan to heterozoan factory turnovers (Wu et al., 2019). Siliciclastic sediment was not present in the carbonate samples obtained from the GP. Seismic profiles show that the GP was far from siliciclastic sediment sources and has been separated from them by deep-water troughs since the Early Miocene (Figures 1; S1). Insufficient siliciclastic input causes the GP to crop out at a depth of hundreds of meters, implying that

terrigenous input is unlikely to be the primary cause of differences in the platform backstepping pattern.

5.3 Volcanic activity and hydrocarbon exploration

Previous studies have documented that magmatic and hydrothermal activities were intense at 5.5 and 2.6 Ma in the flanks of modern carbonate platforms in the northern SCS, resulting in upturned reflectors extending upward to the contemporary sea bottom (Xia et al., 2018; Gao et al., 2019a; Gao et al., 2019b; Sun et al., 2020; Zhao et al., 2021; Gao et al., 2022; Liu G et al., 2023). Submarine volcanoes, magmatic intrusions, and related upward strata extending to the modern seafloor have also been identified by submersible observations and seismic profiles on the flank of the GP (Figures 4, 11), suggesting that contemporaneous

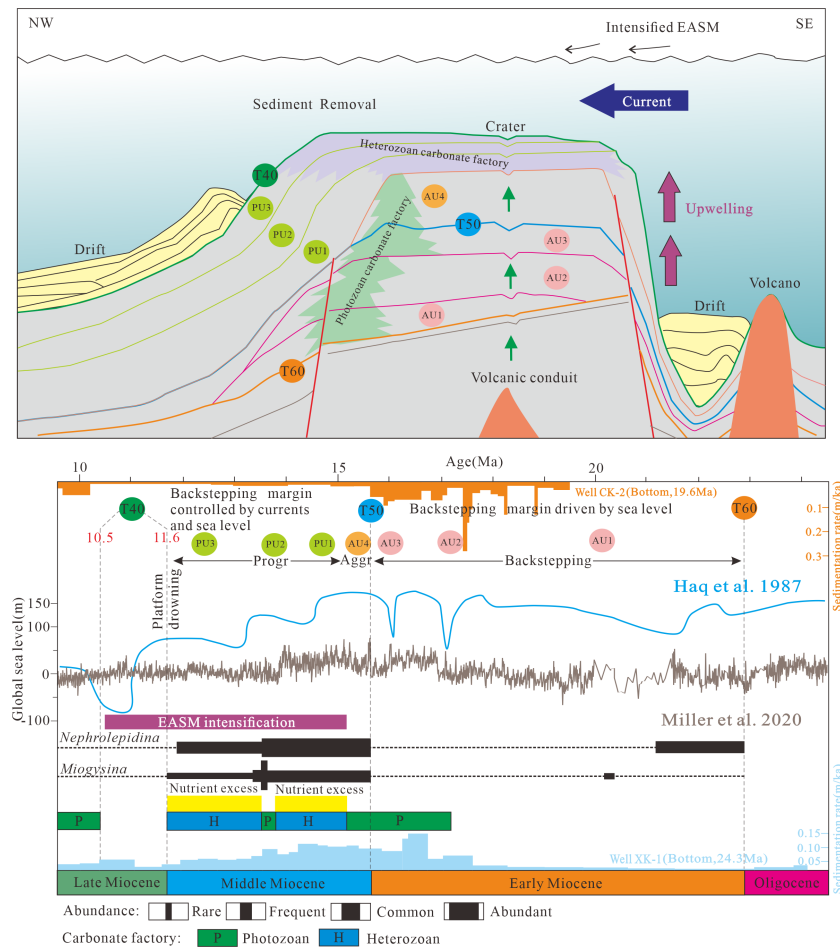


FIGURE 12 Schematic representation of the drowning mechanism at the GP, as proposed here. The sedimentation rate of the Miocene carbonate platform is calculated from wells XK-1 and CK-2 (Yi et al., 2018; Fan et al., 2019). The abundance of benthic foraminifera is referred from Ma et al. (2018). The turnovers of carbonate factory and nutrient excess were recorded in well XK-1 (Wu et al., 2019). Faulting created topography that acted as a template for the initiation of carbonate platform deposition and provided pedestals for the localization of backstepped platforms during AU1–AU3. The concomitant onset of sea-level rise and strong monsoon-related currents enabled the current to flow across the carbonate platform top winnowing and sweeping newly produced sediments off the platform prograding into the basin. Faulting cessation may have instigated progradation of the platform. The gradually drowning steps were accompanied with a reduction of the platform growth rate caused by carbonate factory turnover, leading to the drowning of the platform.

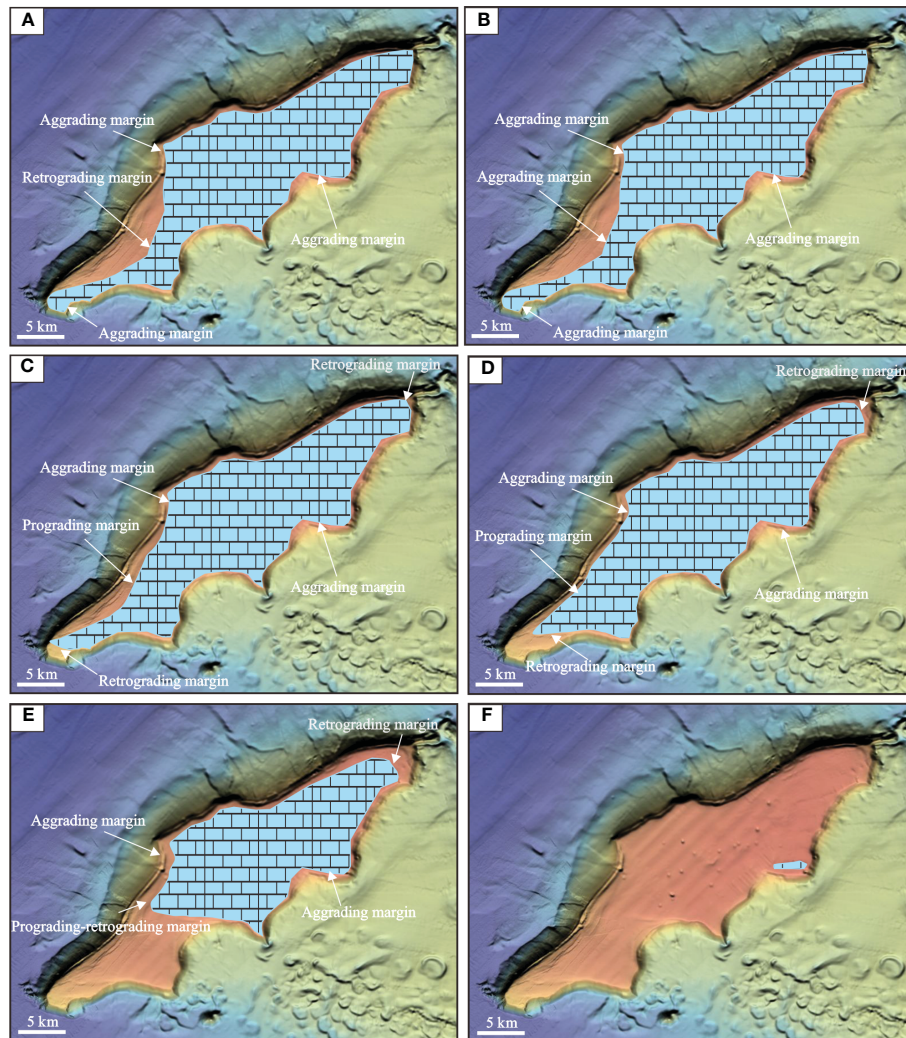


FIGURE 13

Plane distribution of the carbonate platform on the GP illustrating the geologic variation in sequence stacking of coeval platform margins.

(A) Retrograding margin at the southwestern part is most likely controlled by the block tilting during AU3. (B) Most aggrading margins occurred during AU4. (C-E) Prograding margin at the southwestern part represents sediment fluxes to the leeward side of the platform during PU1, PU2, and PU3, coinciding with the asymmetrical backstepping of the platform. Platform backstepped more significantly on the southwestern side of the platform. (F) Representation of the last backstepping phase during the late Middle Miocene.

volcanic activity also occurred there. Interestingly, fluid flow structures, such as pipes and craters, developed in the platform interior, and these pipes penetrated the carbonate platform from the basement (Figure 8). The pipe structure is regarded as a conduit for hydrothermal fluids on the Zhongsha carbonate platform (Huang et al., 2020). Craters on the platform top were created by stratal collapses triggered by hydrothermal fluid erosion. Similar craters have been discovered on the top of the Guangle carbonate platform (Fyhn et al., 2013). The formation and extinction of shallow-water carbonate platforms are assumed to be predominantly governed by tectonic and volcanic activity at volcanic margins; the drowning of ICPs in the Mozambique Channel is such an example (Courgeon et al., 2016). However, carbonate samples from the platform top and flank contain few volcanic fragments, implying that volcanic activity has a limited influence on the diagenetic processes of carbonate

rocks and platform evolution in the GP. Volcanic morphologies, extensive faults, and fracturing networks that exhibit extensional deformation patterns are missing from the GP platform top, implying that platform drowning is unlikely to be caused by extensional deformation.

Previous research has indicated that the heat supplied by magmatism in the basins may induce early hydrocarbon maturation (Gao et al., 2019a). This viewpoint is supported by extensive magmatic intrusion and sills identified beneath the strata of the “Haima” cold seeps in the QDNB (Figure S1). The carbonate sediment produced by the GP was most likely transported into the nearby “Haima” region during the Miocene, improving the reservoir quality of the Miocene strata. Therefore, studying the stratigraphic evolution of the GP could provide new insights into hydrocarbon exploration in the surrounding basins.

TABLE 3 Summary of the platform geometry and carbonate factory in the Cenozoic drowning carbonate platforms.

Drowning time	Platform	Location	platform geometry	Carbonate factory	Drowning mechanisms	Tectonic setting	References
Quaternary	Hawaii reef	Pacific ocean	Backstepping	Photozoan	Sea level, subsidence	Active margin	Webster et al. (2009)
Late Miocene	Guangle platform	South China Sea	Backstepping	Unknown	An increased nutrient supply due to onshore denudation	Passive margin	Fyhn et al. (2013) ; Vu et al. (2017)
Late Miocene	Segitiga Platform	South China Sea	Backstepping	Unknown	Differential subsidence	Passive margin	Bachtel et al. (2004)
Late Middle Miocene	Xuande platform	South China Sea	Asymmetrical backstepping	Heterozoan	Intensified monsoon winds, nutrient excess	Passive margin	Wu et al. (2019) ; Qin et al. (2022)
Late Middle Miocene	Ganquan Plateau	South China Sea	Progradation, asymmetrical Backstepping	Heterozoan	Intensified monsoon winds, nutrient excess	Passive margin	This study
Late Middle Miocene	Maldives	India ocean	Progradation, Backstepping	Heterozoan	Intensified monsoon winds, nutrient excess	Passive margin	Reolid et al. (2020) ; Reolid et al. (2019)
Late Middle Miocene	Northern Marion platform	Northeastern Australia	Progradation, Backstepping	Heterozoan	Intensified monsoon winds, nutrient excess	Passive margin	Isern et al. (2004) ; John and Mutti (2005)
Early Miocene	Yadana platform	Offshore Myanmar, India ocean	Aggradation, Backstepping	Photozoan	Sea level rise, regional tectonic event	Active margin	Paumard et al. (2017)

6 Conclusions

Submersible observations, fossil investigations, and a comprehensive reconstruction of the Miocene seismic facies and geometries of the GP indicate that the platform drowned during the late Middle Miocene. The stratigraphic evolution of the GP can be divided into three distinct stages: (1) platform initiation and structurally controlled retrogradation; (2) platform aggradation and faulting cessation; and (3) platform progradation and backstepping. Platform evolution is susceptible to two major factors: relative sea-level changes and summer monsoon-driven currents. Platform growth could not persist because of the significant subsidence rate throughout the Late Miocene. The asymmetric growth of the GP indicated that the rate of sediment accumulation fluctuated across both space and time, suggesting that stratal patterns in ICPs offer an ambiguous dataset for understanding sea-level changes. The platform geometries were the result of differences in the relative impacts of various parameters on sediment accumulation and the carbonate factory. Tracing the bank-internal geometries and facies demonstrates that the stacking patterns of the GP were vulnerable to wind-driven currents and faulting cessation. Such depositional processes are likely more common in the ICPs of the South China Sea than previously thought. These findings are expected to be applicable to other platforms in the Indo-Pacific region.

Data availability statement

The original contributions presented in the study are included in the article/[Supplementary Material](#). Further inquiries can be directed to the corresponding authors.

Author contributions

YM, SW, DW, CB and WC discussed the initial idea and framework of the manuscript. SW and WC collected samples and wrote the main manuscript text. WC and DW prepared the tables and figures. WC, SW and CB contributed to the discussion of the results, proofing of the manuscript, and review the final version. All authors contributed to the article and approved the submitted version.

Funding

This work was funded by the specific research fund of The Innovation Platform for Academicians of Hainan Province (Grant No. YSPTZX202204), National Key Research and Development Program of China (Grant No. 2021YFC3100601), Shared Voyages Project for Deep-sea and Abyss Scientific Research and Equipment Sea Trials of Hainan Deep-Sea Technology Innovation Center (Grant No. DSTICGXHC-2022002), Hainan Provincial Joint Project of Sanya Yazhou Bay Science and Technology City (Grant No. 2021JLH0047), Hainan Provincial Natural Science Foundation of China (Grant No. 422QN353) and the Postdoctorate Funded Project in Hainan Province.

Acknowledgments

For planning the cruise, we are grateful to Kang Ding, Xiaoteng Peng, Pinxian Wang and Zhimin Jian. We are grateful to the captain

and crew of the R/V Tansuoyihao, the scientific group, the ShenhaiYongshi team, and the Fendouzhe team for their assistance in establishing the sample collection and video recording at sea.

Conflict of interest

Author YM was employed by the company Sinopec.

The remaining authors declare that the research was conducted in the absence of any commercial or financial relationships that could be construed as a potential conflict of interest.

Publisher's note

All claims expressed in this article are solely those of the authors and do not necessarily represent those of their affiliated organizations, or those of the publisher, the editors and the reviewers. Any product that may be evaluated in this article, or claim that may be made by its manufacturer, is not guaranteed or endorsed by the publisher.

References

- Anselmetti, F. S., and Eberli, G. P. (2001). "Sonic velocity in carbonate and a combined product of depositional lithology and diagenetic alterations," in *Subsurface geology of a prograding carbonate platform margin, great bahama bank: results of the Bahamas drilling project*. Ed. R. N. Ginsburg (America, Tulsa:SEPM Society for Sedimentary Geology).
- Aubert, O., and Droxler, A. W. (1996). Seismic stratigraphy and depositional signatures of the maldive carbonate system (Indian ocean). *Mar. Petroleum Geology* 13, 503–536. doi: 10.1016/0264-8172(96)00008-6
- Bachtel, S. L., Kissling, R. D., Martono, D., Rahardjanto, S. P., Dunn, P. A., and MacDonald, B. A. (2004). "Seismic stratigraphic evolution of the Miocene-pliocene segitiga platform, East natuna Sea, Indonesia: the origin, growth, and demise of an isolated carbonate platform," in *Seismic imaging of carbonate reservoirs and systems*. Eds. G. P. Eberli, J. L. Maserferro and J.F.Á.R. Sarg (Seismic Imaging of Carbonate Reservoirs and Systems, America: American Association of Petroleum Geologists).
- Bashir, Y., Faisal, M. A., Biswas, A., Babasafari, A.a., Ali, S. H., Imran, Q. S., et al. (2021). Seismic expression of miocene carbonate platform and reservoir characterization through geophysical approach: application in central luconia, offshore Malaysia. *J. Petroleum Explor. Production Technol.* 11, 1533–1544. doi: 10.1007/s13202-021-01132-2
- Betzler, C., and Eberli, G. P. (2019). Miocene Start of modern carbonate platforms. *Geology* 47, 771–775. doi: 10.1130/G45994.1
- Betzler, C., Eberli, G. P., Lüdmann, T., Reolid, J., Kroon, D., Reijmer, J. J. G., et al. (2018). Refinement of Miocene sea level and monsoon events from the sedimentary archive of the Maldives (Indian ocean). *Prog. Earth Planetary Sci.* 5. doi: 10.1186/s40645-018-0165-x
- Betzler, C., Fürstenau, J., Lüdmann, T., Hübscher, C., Lindhorst, S., Paul, A., et al. (2013). Sea-Level and ocean-current control on carbonate-platform growth, Maldives, Indian ocean. *Basin Res.* 25, 172–196. doi: 10.1111/j.1365-2117.2012.00554.x
- Betzler, C., Hübscher, C., Lindhorst, S., Reijmer, J. J. G., Römer, M., Droxler, A. W., et al. (2009). Monsoon-induced partial carbonate platform drowning (Maldives, Indian ocean). *Geology* 37, 867–870. doi: 10.1130/G25702A.1
- Betzler, C., Lindhorst, S., Lüdmann, T., Reijmer, J. J., Braga, J.-C., Bialik, O. M., et al. (2021). Current and sea level control the demise of shallow carbonate production on a tropical bank (Saya de malha bank, Indian ocean). *Geology* 49, 1431–1435. doi: 10.1130/G49090.1
- Boudagher-Fadel, M. K., and Banner, F. T. (1999). Revision of the stratigraphic significance of the oligocene-miocene "Letter-stages". *Rev. Micropaléontologie* 42, 93–97. doi: 10.1016/S0035-1598(99)90095-8
- Briais, A., Patriat, P., and Tapponnier, P. (1993). Updated interpretation of magnetic anomalies and seafloor spreading stages in the south China Sea: implications for the tertiary tectonics of southeast Asia. *J. Geophysical Research: Solid Earth* 98, 6299–6328. doi: 10.1029/92JB02280
- Chen, W., Huang, X., Wu, S., Liu, G., Wei, H., and Wu, J. (2021). Facies character and geochemical signature in the late quaternary meteoric diagenetic carbonate succession at the xisha islands, south China Sea. *Acta Oceanologica Sin.* 40, 94–111. doi: 10.1007/s13131-021-1713-6
- Clift, P. D., Wan, S., and Blusztajn, J. (2014). Reconstructing chemical weathering, physical erosion and monsoon intensity since 25Ma in the northern south China Sea: a review of competing proxies. *Earth-Science Rev.* 130, 86–102. doi: 10.1016/j.earscirev.2014.01.002
- Courgeon, S., Bachèlery, P., Jouet, G., Jorry, S. J., Bou, E., BouDagher-Fadel, M. K., et al. (2018). The offshore east African rift system: new insights from the sakalaves seamounts (Davie ridge, SW Indian ocean). *Terra Nova* 30, 380–388. doi: 10.1111/ter.12353
- Courgeon, S., Jorry, S. J., Camoin, G. F., BouDagher-Fadel, M. K., Jouet, G., Révillon, S., et al. (2016). Growth and demise of Cenozoic isolated carbonate platforms: new insights from the Mozambique channel seamounts (SW Indian ocean). *Mar. Geology* 380, 90–105. doi: 10.1016/j.margeo.2016.07.006
- El-Yamani, M. S., John, C. M., and Bell, R. (2022). Stratigraphic evolution and karstification of a Cretaceous mid-pacific atoll (Resolution guyot) resolved from core-log-seismic integration and comparison with modern and ancient analogues. *Basin Res.* 34, 1536–1566. doi: 10.1111/bre.12670
- Fan, T., Yu, K., Zhao, J., Jiang, W., Xu, S., Zhang, Y., et al. (2019). Strontium isotope stratigraphy and paleomagnetic age constraints on the evolution history of coral reef islands, northern south China Sea. *GSA Bull.* 132, 803–816. doi: 10.1130/B35088.1
- Flood, P. G. (2001). The 'Darwin point' of pacific ocean atolls and guyots: a reappraisal. *Palaeogeogr. Palaeoclimatol. Palaeoecol.* 175, 147–152. doi: 10.1016/S0031-0182(01)00390-X
- Fyhn, M. B. W., Boldreel, L. O., and Nielsen, L. H. (2009). Tectonic and climatic control on growth and demise of the phanrang karst carbonate platform offshore south Vietnam. *Basin Res.* 21, 225–251. doi: 10.1111/j.1365-2117.2008.00380.x
- Fyhn, M. B. W., Boldreel, L. O., Nielsen, L. H., Giang, T. C., Nga, L. H., Hong, N. T. M., et al. (2013). Carbonate platform growth and demise offshore central Vietnam: effects of early Miocene transgression and subsequent onshore uplift. *J. Asian Earth Sci.* 76, 152–168. doi: 10.1016/j.jseas.2013.02.023
- Gao, J., Bangs, N., Wu, S., Cai, G., Han, S., Ma, B., et al. (2019a). Post-seafloor spreading magmatism and associated magmatic hydrothermal systems in the xisha uplift region, northwestern south China Sea. *Basin Res.* 31, 688–708. doi: 10.1111/bre.12338

Supplementary material

The Supplementary Material for this article can be found online at: <https://www.frontiersin.org/articles/10.3389/fmars.2023.1200788/full#supplementary-material>

SUPPLEMENTARY FIGURE 1

NW–SE seismic section A2 over the continental shelf and slope showing the "Haima" cold seeds and magmatic intrusion in the QDN basin. See Figure 1B and D for the location and legend, respectively. Chaotic or half-transparent reflectivity is evident over most of the QDNB area, suggesting that the mass transport deposits (MTDs) during the deposition of S3 sequence (upper Late Miocene), known also as the Huaguang MTDs documented by Wang et al. (2013), were widely distributed. Purple solid lines in sequence S1 represent the boundary of sub-packages bounded by the unconformities and seismic reflection terminations. See Figure 1B for the location.

SUPPLEMENTARY FIGURE 2

Bathymetric profile across all the craters in the platform; craters are marked by numbers. See Figure 3E for the position of the profile.

SUPPLEMENTARY FIGURE 3

Cross-section through the ICPs on the GU and XU showing the depths of seismic surfaces T40 and T31 penetrated by wells XK-1 and CK-2. See Figure 1B for the location of the cross section. Note that the depths of seismic surfaces are converted from the TWT in the seismic profile crossing the highest basement of the GP and GCP. The seismic profile of GCP is referred from Fyhn et al. (2013).

- Gao, J., Peng, X., Wu, S., Lüdmann, T., McIntosh, K., Ma, B., et al. (2019b). Different expressions of the crustal structure across the dongsha rise along the northeastern margin of the south China Sea. *J. Asian Earth Sci.* 171, 187–200. doi: 10.1016/j.jseas.2018.01.034
- Gao, J., Wu, S., Lüdmann, T., Li, C.-F., Li, L., Lu, Y., et al. (2022). Extensional structures and Cenozoic magmatism in the northwestern south China Sea. *Gondwana Res.* doi: 10.1016/j.gr.2022.09.005
- Halfar, J., Godinez-Orta, L., Mutti, M., Valdez-Holguin, J. E., and Borges, J. M. (2006). Carbonates calibrated against oceanographic parameters along a latitudinal transect in the gulf of California, Mexico. *Sedimentology* 53, 297–320. doi: 10.1111/j.1365-3091.2005.00766.x
- Haq, B. U., Hardenbol, J., and Vail, P. R. (1987). Chronology of fluctuating Sea levels since the Triassic. *Science* 235, 1156–1167. doi: 10.1126/science.235.4793.1156
- Hata, T., Madin, J. S., Cumbo, V. R., Denny, M., Figueiredo, J., Harii, S., et al. (2017). Coral larvae are poor swimmers and require fine-scale reef structure to settle. *Sci. Rep.* 7, 2249. doi: 10.1038/s41598-017-02402-y
- Hendry, J., Burgess, P., Hunt, D., Janson, X., and Zampetti, V. (2021). Seismic characterization of carbonate platforms and reservoirs: an introduction and review. *Geological Society London Special Publications* 509, 1–28. doi: 10.1144/SP509-2021-51
- Hu, J., Kawamura, H., Hong, H., and Qi, Y. (2000). A review on the currents in the south China Sea: seasonal circulation, south China Sea warm current and kuroshio intrusion. *J. Oceanography* 56, 607–624. doi: 10.1023/A:101117531252
- Huang, X., Betzler, C., Wu, S., Bernhardt, A., Eagles, G., Han, X., et al. (2020). First documentation of seismic stratigraphy and depositional signatures of zhongsha atoll (Macclesfield bank), south China Sea. *Mar. Petroleum Geology* 117. doi: 10.1016/j.marpetgeo.2020.104349
- Isern, A. R., Anselmetti, F. S., and Blum, P. (2004). “A neogene carbonate platform, slope, and shelf edifice shaped by Sea level and ocean currents, Marion plateau (Northeast Australia),” in *Seismic imaging of carbonate reservoirs and systems*. Eds. G. P. Eberli, J. L. Masafello and J.F.À.R. Sarg (American Association of Petroleum Geologists).
- Jenkyns, H. C., and Wilson, P. A. (1999). Stratigraphy, paleoceanography, and evolution of Cretaceous pacific guyots: relics from a greenhouse earth. *Am. J. Sci.* 299, 341–392. doi: 10.2475/ajs.299.5.341
- John, C., and Mutti, M. (2005). Relative control of paleoceanography, climate, and eustasy over heterozoan carbonates: a perspective from slope sediments of the Marion plateau (ODP LEG 194). *J. Sedimentary Res.* 75, 216–230. doi: 10.2110/jsr.2005.017
- Li, C.-F., Li, J., Ding, W., Franke, D., Yao, Y., Shi, H., et al. (2015). Seismic stratigraphy of the central south China Sea basin and implications for neotectonics. *J. Geophysical Research: Solid Earth* 120, 1377–1399. doi: 10.1002/2014JB011686
- Ling, A., Eberli, G. P., Swart, P. K., Reolid, J., Stainbank, S., Rüggeberg, A., et al. (2021). Middle Miocene platform drowning in the Maldives associated with monsoon-related intensification of currents. *Palaeogeography Palaeoclimatology Palaeoecol.* 567. doi: 10.1016/j.palaeo.2021.110275
- Liu, G., Wu, S., Gao, J., Zhang, H., Han, X., Qin, Y., et al. (2023). Seismic architecture of yongle isolated carbonate platform in xisha archipelago, south China Sea. *Front. Earth Sci.* 11. doi: 10.3389/feart.2023.1100675
- Liu, Y., Wu, S., Li, X., Chen, W., Han, X., Yang, C., et al. (2023). Seismic stratigraphy and development of a modern isolated carbonate platform (Xuande atoll) in the south China Sea. *Front. Earth Sci.* 10. doi: 10.3389/feart.2022.1042371
- Loo, Y. Y., Billa, L., and Singh, A. (2015). Effect of climate change on seasonal monsoon in Asia and its impact on the variability of monsoon rainfall in southeast Asia. *Geosci. Front.* 6, 817–823. doi: 10.1016/j.gsf.2014.02.009
- Lüdmann, T., Betzler, C., and Lindhorst, S. (2022). The Maldives, a key location of carbonate drifts. *Mar. Geology*, 450, 106838. doi: 10.1016/j.margeo.2022.106838
- Ma, Z.-L., Li, Q.-Y., Liu, X.-Y., Luo, W., Zhang, D.-J., and Zhu, Y.-H. (2018). Palaeoenvironmental significance of Miocene larger benthic foraminifera from the xisha islands, south China Sea. *Palaeoworld* 27, 145–157. doi: 10.1016/j.palwor.2017.05.007
- McNeill, D. F. (2005). Accumulation rates from well-dated late neogene carbonate platforms and margins. *Sedimentary Geology* 175, 73–87. doi: 10.1016/j.sedgeo.2004.12.032
- Meng, M., Yu, K., Hallock, P., Qin, G., Jiang, W., and Fan, T. (2022). Foraminifera indicate neogene evolution of yongle atoll from xisha islands in the south China Sea. *Palaeogeography Palaeoclimatology Palaeoecol.* 602. doi: 10.1016/j.palaeo.2022.111163
- Miller, K. G., Browning, J. V., Schmelz, W. J., Kopp, R. E., Mountain, G. S., and Wright, J. D. (2020). Cenozoic Sea-level and cryospheric evolution from deep-sea geochemical and continental margin records. *Sci. Adv.* 6. doi: 10.1126/sciadv.aaz13
- Mutti, M., and Hallock, P. (2003). Carbonate systems along nutrient and temperature gradients: some sedimentological and geochemical constraints. *Int. J. Earth Sci.* 92, 465–475. doi: 10.1007/s00531-003-0350-y
- Paumard, V., Zuckmeyer, E., Boichard, R., Jorry, S. J., Bourget, J., Borgomano, J., et al. (2017). Evolution of late oligocene - early Miocene attached and isolated carbonate platforms in a volcanic ridge context (Maldives type), yadana field, offshore Myanmar. *Mar. Petroleum Geology* 81, 361–387. doi: 10.1016/j.marpetgeo.2016.12.012
- Petrovic, A., Lüdmann, T., Afifi, A. M., Saitz, Y., Betzler, C., and Vahrenkamp, V. (2023). Fragmentation, rafting, and drowning of a carbonate platform margin in a rift-basin setting. *Geology*. doi: 10.1130/G50546.1
- Qin, Y., Wu, S., and Betzler, C. (2022). Backstepping patterns of an isolated carbonate platform in the northern south China Sea and its implication for paleoceanography and paleoclimate. *Mar. Petroleum Geology* 146. doi: 10.1016/j.marpetgeo.2022.105927
- Reolid, J., Betzler, C., Braga, J. C., Lüdmann, T., Ling, A., and Eberli, G. P. (2020). Facies and geometry of drowning steps in a Miocene carbonate platform (Maldives). *Palaeogeography Palaeoclimatology Palaeoecol.* 538. doi: 10.1016/j.palaeo.2019.109455
- Reolid, J., Betzler, C., Lüdmann, T., and Eberli, G. (2019). Facies and sedimentology of a carbonate delta drift (Miocene, Maldives). *Sedimentology* 66, 1243–1265. doi: 10.1111/sed.12575
- Sattler, U., Immenhauser, A., Schlager, W., and Zampetti, V. (2009). Drowning history of a Miocene carbonate platform (Zhujiang formation, south China Sea). *Sedimentary Geology* 219, 318–331. doi: 10.1016/j.sedgeo.2009.06.001
- Schlager, W. (1981). The paradox of drowned reefs and carbonate platforms. *Geological Soc. America Bull.* 92, 197–211. doi: 10.1130/0016-7606(1981)92<197:TPODRA>2.0.CO;2
- Schlager, W. (2000). “Sedimentation rates and growth potential of tropical, cool-water and mud-mound carbonate systems,” in *Carbonate platform systems: components and interactions*. Eds. E. Insalaco, P. W. Skelton and T. J. Palmer (England, London: Geological Society of London).
- Shao, L., Cui, Y., Qiao, P., Zhang, D., Liu, X., and Zhang, C. (2017). Sea-Level changes and carbonate platform evolution of the xisha islands (South China Sea) since the early Miocene. *Palaeogeography Palaeoclimatology Palaeoecol.* 485, 504–516. doi: 10.1016/j.palaeo.2017.07.006
- Staudigel, H., and Clague, D. A. (2010). The geological history of deep-sea volcanoes biosphere, hydrosphere, and lithosphere interactions. *Oceanography* 23, 58–71. doi: 10.5670/oceanog.2010.62
- Sun, Q., Alves, T. M., Zhao, M., Sibuet, J.-C., Gêrôme, C., and Xie, X. (2020). Post-rift magmatism on the northern south China Sea margin. *GSA Bull.* 132, 2382–2396. doi: 10.1130/B35471.1
- Sun, Z., Zhou, D., Zhong, Z., Zeng, Z., and Wu, S. (2003). Experimental evidence for the dynamics of the formation of the yinggehai basin, NW south China Sea. *Tectonophysics* 372, 41–58. doi: 10.1016/S0040-1951(03)00230-0
- Vu, A. T., Wessel Fyhn, M. B., Xuan, C. T., Nguyen, T. T., Hoang, D. N., Pham, L. T., et al. (2017). Cenozoic Tectonic and stratigraphic development of the central Vietnamese continental margin. *Mar. Petroleum Geology* 86, 386–401. doi: 10.1016/j.marpetgeo.2017.06.001
- Wang, J., Wu, S., Kong, X., Ma, B., Li, W., Wang, D., et al. (2018). Subsurface fluid flow at an active cold seep area in the qiongdongnan basin, northern south China Sea. *J. Asian Earth Sci.* 168, 17–26. doi: 10.1016/j.jseas.2018.06.001
- Wang, D., Wu, S., Qin, Z., Spence, G., and Lü, F. (2013). Seismic characteristics of the huaguang mass transport deposits in the qiongdongnan basin, south China Sea: implications for regional tectonic activity. *Mar. Geology* 346, 165–182. doi: 10.1016/j.margeo.2013.09.003
- Wang, R., Yu, K., Jones, B., Wang, Y., Zhao, J., Feng, Y., et al. (2018). Evolution and development of Miocene “island dolostones” on xisha islands, south China Sea. *Mar. Geology* 406, 142–158. doi: 10.1016/j.margeo.2018.09.006
- Wang, H., Zhao, Q., Wu, S., Wang, D., and Wang, B. (2018). Post-rifting magmatism and the drowned reefs in the xisha archipelago domain. *J. Ocean Univ. China* 17, 195–208. doi: 10.1007/s11802-018-3485-y
- Webster, J. M., Braga, J. C., Clague, D. A., Gallup, C., Hein, J. R., Potts, D. C., et al. (2009). Coral reef evolution on rapidly subsiding margins. *Global Planetary Change* 66, 129–148. doi: 10.1016/j.gloplacha.2008.07.010
- Wilson, P. A., Jenkyns, H. C., Elderfield, H., and Larson, R. L. (1998). The paradox of drowned carbonate platforms and the origin of Cretaceous pacific guyots. *Nature* 392, 889–894. doi: 10.1038/31865
- Wu, F., Xie, X., Li, X., Betzler, C., Shang, Z., and Cui, Y. (2019). Carbonate factory turnovers influenced by the monsoon (Xisha islands, south China Sea). *J. Geological Soc.* 176, 885–897. doi: 10.1144/jgs2018-086
- Wu, F., Xie, X., Zhu, Y., Chen, B., and Shang, Z. (2021a). Sequence stratigraphy of the late oligocene carbonate system on the xisha islands in the south China Sea. *Int. J. Earth Sci.* 110, 1611–1629. doi: 10.1007/s00531-021-02033-9
- Wu, F., Xie, X., Zhu, Y., Coletti, G., Betzler, C., Cui, Y., et al. (2021b). Early development of carbonate platform (Xisha islands) in the northern south China Sea. *Mar. Geology* 441. doi: 10.1016/j.margeo.2021.106629
- Wu, S., Chen, W., Huang, X., Liu, G., Li, X., and Betzler, C. (2020). Facies model on the modern isolated carbonate platform in the xisha archipelago, south China Sea. *Mar. Geology* 425. doi: 10.1016/j.margeo.2020.106203
- Wu, S., Yang, Z., Wang, D., Lü, F., Lüdmann, T., Fulthorpe, C., et al. (2014). Architecture, development and geological control of the xisha carbonate platforms, northwestern south China Sea. *Mar. Geology* 350, 71–83. doi: 10.1016/j.margeo.2013.12.016
- Wu, S., Zhang, H., Qin, Y., Chen, W., Liu, G., and Han, X. (2022). Seismic imaging and 3D architecture of yongle atoll of the xisha archipelago, south China Sea. *Acta Geologica Sin. - English Edition* 96, 1778–1791. doi: 10.1111/1755-6724.14892
- Xia, S., Zhao, F., Zhao, D., Fan, C., Wu, S., Mi, L., et al. (2018). Crustal plumbing system of post-rift magmatism in the northern margin of south China Sea: new insights

from integrated seismology. *Tectonophysics* 744, 227–238. doi: 10.1016/j.tecto.2018.07.002

Xie, S.-P. (2003). Summer upwelling in the south China Sea and its role in regional climate variations. *J. Geophysical Res.* 108. doi: 10.1029/2003JC001867

Xie, X., Müller, R. D., Ren, J., Jiang, T., and Zhang, C. (2008). Stratigraphic architecture and evolution of the continental slope system in offshore hainan, northern south China Sea. *Mar. Geology* 247, 129–144. doi: 10.1016/j.margeo.2007.08.005

Yang, Y., Yu, K., Wang, R., Fan, T., Jiang, W., Xu, S., et al. (2022). $^{87}\text{Sr}/^{86}\text{Sr}$ of coral reef carbonate strata as an indicator of global sea level fall: evidence from a 928.75-m-long core in the south China Sea. *Mar. Geology* 445.

Yi, L., Jian, Z., Liu, X., Zhu, Y., Zhang, D., Wang, Z., et al. (2018). Astronomical tuning and magnetostratigraphy of neogene biogenic reefs in xisha islands, south China Sea. *Sci. Bull.* 63, 564–573. doi: 10.1016/j.scib.2018.04.001

Zachos, J., Pagani, M., Sloan, L., Thomas, E., and Billups, K. (2001). Trends, rhythms, and aberrations in global climate 65 ma to present. *Science* 292, 686–693. doi: 10.1126/science.1059412

Zampetti, V., Schlager, W., van Konijnenburg, J.-H., and Everts, A.-J. (2004). Architecture and growth history of a Miocene carbonate platform from 3D seismic reflection data; luconia province, offshore Sarawak, Malaysia. *Mar. Petroleum Geology* 21, 517–534. doi: 10.1016/j.marpetgeo.2004.01.006

Zhao, F., Berndt, C., Alves, T. M., Xia, S., Li, L., Mi, L., et al. (2021). Widespread hydrothermal vents and associated volcanism record prolonged Cenozoic magmatism in the south China Sea. *GSA Bull.* 133, 2645–2660. doi: 10.1130/B35897.1

Zhao, Q. H., Jian, Z. M., Wang, J. L., Cheng, X. R., Huang, B. Q., Xu, J., et al. (2001). Neogene oxygen isotopic stratigraphy, ODP site 1148, northern south China Sea. *Sci. China Ser. D-Earth Sci.* 44, 934–942. doi: 10.1007/BF02907086

Zhao, Z., Sun, Z., Sun, L., Wang, Z., and Sun, Z. (2018). Cenozoic Tectonic subsidence in the qiongdongnan basin, northern south China Sea. *Basin Res.* 30, 269–288. doi: 10.1111/bre.12220